J. Fluid Mech. (1994), *vol.* 277, *pp.* 197–225

Optimal energy density growth in Hagen–Poiseuille flow

By PETER J. SCHMID[1]† AND DAN S. HENNINGSON[2]

[1] Department of Mathematics, Massachusetts Institute of Technology, Cambridge, MA 02139, USA

[2] Aeronautical Research Institute of Sweden (FFA), Box 11021, S-16111 Bromma, Sweden *and* Department of Mechanics, Royal Institute of Technology, S-10044 Stockholm, Sweden

(Received 9 February 1993 and in revised form 15 March 1994)

Linear stability of incompressible flow in a circular pipe is considered. Use is made of a vector function formulation involving the radial velocity and radial vorticity only. Asymptotic as well as transient stability are investigated using eigenvalues and ϵ-pseudoeigenvalues, respectively. Energy stability is probed by establishing a link to the numerical range of the linear stability operator. Substantial transient growth followed by exponential decay has been found and parameter studies revealed that the maximum amplification of initial energy density is experienced by disturbances with no streamwise dependence and azimuthal wavenumber $n = 1$. It has also been found that the maximum in energy scales with the Reynolds number squared, as for other shear flows. The flow field of the optimal disturbance, exploiting the transient growth mechanism maximally, has been determined and followed in time. Optimal disturbances are in general characterized by a strong shear layer in the centre of the pipe and their overall structure has been found not to change significantly as time evolves. The presented linear transient growth mechanism which has its origin in the non-normality of the linearized Navier–Stokes operator, may provide a viable process for triggering finite-amplitude effects.

1. Introduction

The onset of turbulent fluid motion in a circular pipe has been the object of many investigations over the past few decades. This type of flow is of particular interest since no critical Reynolds number exists above which solutions grow exponentially. This has been shown analytically for axisymmetric disturbances (Romanov 1973; Herron 1991), whereas for non-axisymmetric perturbations there exists a large body of numerical evidence that suggests that Poiseuille flow in a circular pipe is linearly stable for all Reynolds numbers (Lessen, Sadler & Liu 1968; Metcalfe & Orszag 1973; Salwen, Cotton & Grosch 1980). Experimental investigations, however, show that pipe flow accommodates growing perturbations for Reynolds numbers (based on the pipe radius and the centreline velocity) larger than approximately 2000 (Salwen *et al.* 1980). Although several investigators have tried to resolve this discrepancy between the linear theory and the experiments, the hydrodynamic stability problem for circular pipe flow still lacks a satisfactory explanation.

Davey (1978) considered the linear stability of flow in an elliptical pipe which is nearly circular. The resulting perturbation problem was solved for the required

† Present address: Department of Applied Mathematics, University of Washington, Seattle, WA 98195, USA.

eccentricity of the pipe necessary to destabilize the mean flow. Above an ellipticity of $e = 0.07$ exponentially growing solutions have been found. His analysis also showed that the temporal damping rates of non-axisymmetric wall modes monotonically decrease as the eccentricity of the pipe increases.

Mackrodt (1976) studied the effect of rigid rotation on the stability of circular pipe flow and found that for high axial Reynolds numbers, only a small amount of rotation is required to trigger instabilities that may ultimately lead to transition. In an earlier investigation Maslowe (1974) derived a necessary condition for non-axisymmetric instabilities in rigidly rotating flows based on the stability equations given in Howard & Gupta (1962).

In a similar attempt, Tatsumi (1952) investigated the linear stability of the inlet flow of a circular pipe and determined the critical Reynolds number for this type of flow to be about 9700.

Nonlinear effects have also been proposed as a reason for the discrepancy between linear theory and experiment. Davey & Nguyen (1971) calculated the stability of pipe flow to small but finite-amplitude axisymmetric disturbances. Their weakly nonlinear analysis showed that a centre mode rather than a wall mode is more likely to cause nonlinear instabilities.

Gustavsson (1989) analysed the linear stability operator in terms of degeneracies between the pressure perturbations and the streamwise velocity perturbations. The resulting resonance may lead to algebraic growth followed by exponential decay. This resonance has been proposed as a possible mechanism that triggers nonlinear effects.

It has been recognized in recent years that the linear stability operators for plane shear flows can support solutions that exhibit large transient growth in energy, although the eigensolutions of the operators are damped. This phenomenon is due to the non-normality of the underlying linear operator, which results in a set of non-orthogonal eigenfunctions. Expansions of the flow field in non-orthogonal eigenfunctions can result in large expansion coefficients that mostly cancel each other out. As time progresses, however, this cancellation ceases to exist, resulting in transient growth of initial energy.

This transient growth mechanism has attracted the attention of scientists in the field of hydrodynamic stability. Farrell (1988) studied the development of two-dimensional disturbances that optimally excite plane channel flow by this linear mechanism and computed the amplification factors of their energy density. Gustavsson (1991), however, who considered the energy growth of three-dimensional disturbances for various parameter combinations, showed that the growth of energy density for three-dimensional disturbances can be substantially larger than that for two-dimensional perturbations. Subsequent studies have been undertaken by Butler & Farrell (1992), who used a variational technique to calculate the optimal disturbances, and by Reddy, Schmid & Henningson (1993) and Reddy & Henningson (1993) who directly estimated the matrix exponential in order to explain and quantify transient effects in plane Poiseuille flow for two- and three-dimensional perturbations.

Trefethen *et al.* (1993) addressed the general concept of non-modal stability analysis and, besides the transient growth of disturbance energy, gave two alternative interpretations of non-modal effects: the resonance behaviour with background noise and the sensitivity to laboratory imperfections.

The nonlinear development of disturbances experiencing transient growth was first studied in a magnetohydrodynamical context by Willke (1967). He found that a finite-amplitude disturbance can at most grow up to the magnitude of the maximum velocity difference present in the base flow (see Lundbladh 1993 for a further discussion of the

implications of this work for wall-bounded shear flows). Boberg & Brosa (1988) investigated the nonlinear initial value problem for flow in a pipe. They suggested a linear non-modal mechanism consisting of decaying and transiently amplified solutions of the linearized problem as a main provider of kinetic disturbance energy. The severe truncation of their modal expansion and the exclusion of the mean flow modification, however, do not allow immediate and quantitative conclusions about the onset of pipe flow turbulence, although some stability features have been captured qualitatively. In a report by O'Sullivan & Breuer (1992), transient growth of disturbance energy for a specific family of initial conditions has been observed and quantitatively mapped out for a range of parameters. In a similar attempt, Bergström (1992, 1993) documented transient effects in circular pipes for vanishing streamwise wavenumbers (1992) as well as for a range of non-zero streamwise wavenumbers (1993).

As in the investigations just mentioned, the present work extends the scope of linear theory for circular pipe flow to include *transient* behaviour of infinitesimal three-dimensional disturbances. It is restricted to the linear growth mechanism described above. In addition to what has previously been done, an exhaustive parameter study of the transient growth is presented. Furthermore, we focus on the structure of the disturbances that achieve the maximum amplification of initial energy density.

A similar analysis of transient phenomena for plane Poiseuille and plane Couette flow has been presented in Reddy & Henningson (1993), and the structure of this presentation will closely follow their work. The mathematical methods will be adapted to the flow in circular geometries, and similarities as well as discrepancies between the two flow geometries will be pointed out and investigated.

The organization of the paper is as follows. Section 2 states the governing equations; use is made of a two-component vector formulation involving the radial velocity and the radial vorticity, in analogy to a similar decomposition technique for plane bounded flows. A scalar product and its associated norm based on the energy density of the flow are introduced and the necessary tools to characterize the transient behaviour of solutions to the initial value problem will be developed. In §3 we consider the asymptotic time behaviour of the eigenvalues of the linear stability operator, as well as the transient time behaviour as described by methods introduced in §2. Furthermore, the issue of optimal disturbances for circular pipe flow is addressed and a parameter study mapping out the transient energy density growth is presented. Section 4 concludes this work with a discussion of the results presented.

2. The initial value problem

In this section we will state the governing equations and develop the mathematical framework to analyse the linear initial value problem for the evolution of infinitesimal disturbances in incompressible pipe flow. As an aid to the reader, the analysis of a simple model problem using the techniques outlined in this section is provided in the Appendix to complement the analysis of the linearized Navier–Stokes operator for flow in circular pipes.

2.1. *Linearized Navier–Stokes equations*

Our starting point for the analysis of infinitesimal disturbances in circular pipe flow is the linearized Navier–Stokes equation for incompressible flow in circular coordinates, where an axial mean flow of the form $U = U(r)$ has been assumed:

$$\frac{\partial u}{\partial t}+U\frac{\partial u}{\partial z}+vU'=-\frac{\partial p}{\partial z}+\frac{1}{Re}\left[\frac{1}{r}\frac{\partial}{\partial r}\left(r\frac{\partial u}{\partial r}\right)+\frac{1}{r^2}\frac{\partial^2 u}{\partial\theta^2}+\frac{\partial^2 u}{\partial z^2}\right],$$

$$\frac{\partial v}{\partial t}+U\frac{\partial v}{\partial z}=-\frac{\partial p}{\partial r}+\frac{1}{Re}\left[\frac{1}{r}\frac{\partial}{\partial r}\left(r\frac{\partial v}{\partial r}\right)+\frac{1}{r^2}\frac{\partial^2 v}{\partial\theta^2}+\frac{\partial^2 v}{\partial z^2}-\frac{v}{r^2}-\frac{2}{r^2}\frac{\partial w}{\partial\theta}\right],$$

$$\frac{\partial w}{\partial t}+U\frac{\partial w}{\partial z}=-\frac{1}{r}\frac{\partial p}{\partial\theta}+\frac{1}{Re}\left[\frac{1}{r}\frac{\partial}{\partial r}\left(r\frac{\partial w}{\partial r}\right)+\frac{1}{r^2}\frac{\partial^2 w}{\partial\theta^2}+\frac{\partial^2 w}{\partial z^2}+\frac{2}{r^2}\frac{\partial v}{\partial\theta}-\frac{w}{r^2}\right],$$

$$\frac{\partial u}{\partial z}+\frac{1}{r}\frac{\partial(rv)}{\partial r}+\frac{1}{r}\frac{\partial w}{\partial\theta}=0.$$

Here u, v, w are the perturbation velocities in the axial (z), radial (r) and the azimuthal (θ) direction, respectively; p denotes the perturbation pressure and the prime stands for a differentiation with respect to r. The equations above have been non-dimensionalized by the pipe radius a and the centreline velocity U_{CL}, and the Reynolds number R is defined as $U_{CL}a/\nu$, with ν the kinematic viscosity. As the flow is periodic in the azimuthal direction and will be assumed periodic in the streamwise direction, the dependence of all flow quantities on these coordinates will be taken to be of the form $(u,v,w,p)^T=(\hat{u},\hat{v},\hat{w},\hat{p})^T\exp(\mathrm{i}\alpha z+\mathrm{i}n\theta)$ with $\alpha\in\mathscr{R}$ as the streamwise wavenumber and $n\in\mathscr{Z}$ as the azimuthal wavenumber. The presence of two homogeneous directions allows us to further reduce the equations to the more convenient radial velocity ($\hat{v}$)–radial vorticity ($\hat{\eta}$) form as suggested by Burridge & Drazin (1969)

$$\left(R\frac{\partial}{\partial t}+\mathrm{i}\alpha RU\right)\mathscr{T}\hat{\Phi}-\frac{\mathrm{i}\alpha R}{r}\left(\frac{U'}{k^2r}\right)'\hat{\Phi}=\mathscr{T}(k^2r^2\mathscr{T})\hat{\Phi}+2\alpha Rn^2\mathscr{T}\hat{\Omega},$$

$$k^2r^2\left(R\frac{\partial}{\partial t}+\mathrm{i}\alpha RU\right)\hat{\Omega}+\frac{\mathrm{i}U'}{r}\hat{\Phi}=\mathscr{S}\hat{\Omega}+\frac{2\alpha R}{R^2}\mathscr{T}\hat{\Phi},$$

with

$$k^2=\alpha^2+n^2/r^2,$$

$$\mathscr{T}=\frac{1}{r^2}-\frac{1}{r}\frac{\mathrm{d}}{\mathrm{d}r}\left(\frac{1}{k^2r}\frac{\mathrm{d}}{\mathrm{d}r}\right),\qquad \mathscr{S}=k^4r^2-\frac{1}{r}\frac{\mathrm{d}}{\mathrm{d}r}\left(k^2r^3\frac{\mathrm{d}}{\mathrm{d}r}\right),$$

$$\hat{\Phi}\equiv-\mathrm{i}r\hat{v},\quad \hat{\Omega}\equiv\frac{\alpha r\hat{w}-n\hat{u}}{nRk^2r^2}=\frac{\hat{\eta}}{\mathrm{i}nRk^2r}.$$

The variables $\hat{\Phi}$ and $\hat{\Omega}$ describe the problem completely; the streamwise velocity $\hat{u}$ and the azimuthal velocity $\hat{w}$ can be recovered by

$$\hat{u}=-\frac{\alpha}{k^2r}\frac{\partial\hat{\Phi}}{\partial r}-n^2R\hat{\Omega},\quad \hat{w}=-\frac{n}{k^2r^2}\frac{\partial\hat{\Phi}}{\partial r}+\alpha Rnr\hat{\Omega},$$

where the continuity equation and the definition of the radial vorticity have been exploited.

In the equation stated above a similar scaling has been used as proposed by Gustavsson (1991) for plane Poiseuille flow. This scaling has the advantage that for two-dimensional disturbances ($\alpha=0$), the equations only depend on the azimuthal wavenumber n if the scaled time $\tau=t/R$ is introduced. Hence, for a given azimuthal periodicity, results obtained for a particular Reynolds number can be scaled to a different Reynolds number in a straightforward manner. For the general case of three-dimensional perturbations, three parameters have to be specified, which are most conveniently chosen to be αR, R and n.

For the subsequent analysis it will be of advantage to cast the governing equations into matrix form by introducing vector functions $\boldsymbol{q} = (\hat{\Phi}\ \hat{\Omega})^T$, which results in the linear initial-boundary-value problem

$$\mathscr{L}\boldsymbol{q} + \frac{\partial}{\partial \tau}\mathscr{M}\boldsymbol{q} = 0, \tag{1a}$$

with

$$\mathscr{L} = \begin{pmatrix} \mathrm{i}\alpha R U\mathscr{T} - \mathrm{i}\dfrac{\alpha R}{r}\left(\dfrac{U'}{k^2 r}\right)' - \mathscr{T}(k^2 r^2 \mathscr{T}) & 2\alpha R n^2 \mathscr{T} \\ -\mathrm{i}\dfrac{U'}{r} - \dfrac{2\alpha R}{R^2}\mathscr{T} & \mathrm{i}\alpha R k^2 r^2 U - \mathscr{S} \end{pmatrix}, \tag{1b}$$

$$\mathscr{M} = \begin{pmatrix} \mathscr{T} & 0 \\ 0 & k^2 r^2 \end{pmatrix}, \quad \boldsymbol{q} = \begin{pmatrix} \hat{\Phi} \\ \hat{\Omega} \end{pmatrix}. \tag{1c, d}$$

In addition to the inviscid coupling term $-\mathrm{i}U'/r$, which in an analogous form is also present in plane flows (Henningson & Schmid 1992), viscous coupling terms appear which stem from the non-zero off-diagonal terms in the vector Laplacian for cylindrical coordinate systems.

Note that the linear evolution operator, mapping the flow field to its time derivative, is in this notation given by $\mathscr{L}_1 = \mathscr{M}^{-1}\mathscr{L}$.

The matrix formulation for hydrodynamic stability equations with two homogeneous coordinates was originally introduced by DiPrima (1967) in an analysis of Taylor–Couette flow. It has been applied to bounded parallel shear flows by Henningson & Schmid (1992), where it has proven advantageous for analytical studies and numerical implementations.

Boundary conditions have to be imposed on $\hat{\Phi}$ and $\hat{\Omega}$ in order to uniquely determine the solution to the physical problem. The boundary conditions for the solid wall at $r = 1$ are given by the no-slip assumption and can be written in the form

$$\hat{\Phi} = \hat{\Phi}' = \hat{\Omega} = 0 \quad \text{at} \quad r = 1. \tag{2}$$

The boundary conditions for the channel centreline ($r = 0$) can easily be derived using the fact that the velocity vector has a vanishing azimuthal dependence as the centreline is approached (Khorrami, Malik & Ash 1989), i.e.

$$\lim_{r\to 0}\frac{\partial}{\partial\theta}(u\boldsymbol{e}_z + v\boldsymbol{e}_r + w\boldsymbol{e}_\theta) = 0,$$

where $\boldsymbol{e}_z$, $\boldsymbol{e}_r$, $\boldsymbol{e}_\theta$ denote the unit vectors in the axial, radial and azimuthal directions, respectively. For cylindrical coordinates

$$\frac{\partial \boldsymbol{e}_z}{\partial\theta} = 0, \quad \frac{\partial \boldsymbol{e}_r}{\partial\theta} = \boldsymbol{e}_\theta, \quad \frac{\partial \boldsymbol{e}_\theta}{\partial\theta} = -\boldsymbol{e}_r,$$

and the restriction that each individual component has to vanish yields the required boundary conditions for Φ and $\hat{\Omega}$ at $r = 0$:

$$\left.\begin{array}{lll} \hat{\Phi} = \hat{\Phi}' = 0 & \text{for} & n = 0, \\ \hat{\Phi} = \hat{\Omega} = 0, \quad \hat{\Phi}' \text{ finite} & \text{for} & n = \pm 1, \\ \hat{\Phi} = \hat{\Phi}' = \hat{\Omega} = 0 & \text{for} & n \geqslant 2. \end{array}\right\} \tag{3}$$

The governing equation (1) together with the boundary conditions (2) and (3) fully describe the motion of infinitesimal spatially periodic disturbances and will be the focus of further analysis.

2.2. *Inner product, associated norm and eigenfunction expansion*

As we are mainly interested in an analysis of the initial value problem rather than just the eigenvalues of the evolution operator ($\mathscr{L}_1$), it is necessary to introduce a scalar product upon which all further computations will rest. This scalar product and its associated norm constitute the fundamental measure for quantities describing the transient behaviour. Both the qualitative and quantitative behaviour will depend on the choice of the scalar product.

For the remainder of this presentation we will make use of a scalar product based on the energy density defined as

$$(\boldsymbol{q}_1, \boldsymbol{q}_2)_{\mathscr{M}} = (\mathscr{M}\boldsymbol{q}_1, \boldsymbol{q}_2)_2 = \pi \int_0^1 \left[\frac{\hat{\Phi}_1' \hat{\Phi}_2^{*\prime}}{k^2 r^2} + \frac{\hat{\Phi}_1 \hat{\Phi}_2^*}{r^2} + k^2 r^2 n^2 R^2 \hat{\Omega}_1 \hat{\Omega}_2^* \right] r \, \mathrm{d}r, \tag{4}$$

where the L_2-scalar product $(.,.)_2$ is defined as

$$(f, g) = (g, f)^* = \pi \int_0^1 g^H f r \, \mathrm{d}r.$$

The superscripts H and $*$ denote the complex-conjugate transpose and the complex conjugate, respectively.

Based on this scalar product, the associated norm, referred to hereafter as the energy norm, is given as follows:

$$\begin{aligned} \|\boldsymbol{q}\|_{\mathscr{M}}^2 = (\boldsymbol{q}, \boldsymbol{q})_{\mathscr{M}} = (\mathscr{M}\boldsymbol{q}, \boldsymbol{q})_2 &= \pi \int_0^1 \left[\frac{|\hat{\Phi}'|^2}{k^2 r^2} + \frac{|\hat{\Phi}|^2}{r^2} + k^2 r^2 n^2 R^2 |\hat{\Omega}|^2 \right] r \, \mathrm{d}r \\ &= \pi \int_0^1 [|\hat{u}|^2 + |\hat{v}|^2 + |\hat{w}|^2] r \, \mathrm{d}r; \end{aligned}$$

$\|\boldsymbol{q}\|_{\mathscr{M}}^2$ is the kinetic energy density for flow in circular geometry.

It will greatly simplify our further analysis to use a discrete approximation of the continuous scalar product defined by (4). This is most easily accomplished by an expansion of the vector quantities $\boldsymbol{q}$ in the vector eigensolutions of the linear initial value problem. Assuming solutions of the form

$$\boldsymbol{q} = \tilde{\boldsymbol{q}} \exp(-\mathrm{i}\omega\tau) \quad \omega \in \mathscr{C}$$

will transform the initial value problem (1) into a generalized eigenvalue problem of the form

$$\mathscr{L}\tilde{\boldsymbol{q}} = \mathrm{i}\omega\mathscr{M}\tilde{\boldsymbol{q}}. \tag{5}$$

Restricting ourselves to the space $\mathscr{S}^N$ spanned by the first N eigenfunctions of (5)

$$\mathscr{S}^N = \mathrm{span}\{\tilde{\boldsymbol{q}}_1, \tilde{\boldsymbol{q}}_2, \ldots, \tilde{\boldsymbol{q}}_N\}$$

and expanding the vector functions $\boldsymbol{q} \in \mathscr{S}^N$ in the basis $\{\tilde{\boldsymbol{q}}_1, \ldots, \tilde{\boldsymbol{q}}_N\}$,

$$\boldsymbol{q} = \sum_{n=1}^{N} \kappa_n(\tau) \tilde{\boldsymbol{q}}_n \quad \boldsymbol{q} \in \mathscr{S}^N, \tag{6}$$

we can restate the initial value problem (1) in a particularly simple form as

$$\frac{\mathrm{d}\boldsymbol{\kappa}}{\mathrm{d}\tau} = -\mathrm{i}\boldsymbol{\Lambda}\boldsymbol{\kappa}, \quad \boldsymbol{\Lambda} \in \mathscr{C}^{N\times N}, \quad \boldsymbol{\kappa} \in \mathscr{C}^N, \tag{7}$$

with $$\boldsymbol{\kappa} = (\kappa_1, \kappa_2, \ldots, \kappa_N)^T, \quad \boldsymbol{\Lambda} = \operatorname{diag}\{\omega_1, \omega_2, \ldots, \omega_N\}.$$

Thus, $\boldsymbol{\Lambda}$ represents the linear evolution operator, $\mathscr{L}_1$, projected onto the space $\mathscr{S}^N$. Henceforth, we can focus our attention on the analysis of the initial value problem (7) and describe the evolution of infinitesimal disturbances in circular pipe flow by the expansion coefficients κ instead of the state vector $\boldsymbol{q}$. For later comparison with results obtained by previous investigators we also define the spectrum $\boldsymbol{\Lambda}_R$ as $\boldsymbol{\Lambda}_R = (1/R)\operatorname{diag}\{\omega_1, \omega_2, \ldots, \omega_N\}$.

To complete the transformation from the vector quantities $\boldsymbol{q}$ to the expansion coefficients κ, we also have to reformulate the scalar product as well as its associated norm.

If $\boldsymbol{q}_1, \boldsymbol{q}_2 \in \mathscr{S}^N$, it follows from (4) and (6) that

$$(\boldsymbol{q}_1, \boldsymbol{q}_2)_{\mathscr{M}} = \pi \int_0^1 \boldsymbol{q}_2^H \mathscr{M} \boldsymbol{q}_1 \, r \, \mathrm{d}r = \boldsymbol{\kappa}_2^H \boldsymbol{M} \boldsymbol{\kappa}_1, \quad \boldsymbol{M} \in \mathscr{C}^{N \times N},$$

where $\boldsymbol{M}$ is the Hermitian matrix whose elements are given by

$$M_{ij} = (\tilde{\boldsymbol{q}}_i, \tilde{\boldsymbol{q}}_j)_{\mathscr{M}} = \pi \int_0^1 \tilde{\boldsymbol{q}}_j^H \mathscr{M} \tilde{\boldsymbol{q}}_i \, r \, \mathrm{d}r.$$

After factoring $\boldsymbol{M}$ according to $\boldsymbol{M} = \boldsymbol{F}^H \boldsymbol{F}$, the vector scalar product $(.,.)_{\boldsymbol{M}}$ can be defined as

$$(\boldsymbol{\kappa}_1, \boldsymbol{\kappa}_2)_{\boldsymbol{M}} = (\boldsymbol{F}\boldsymbol{\kappa}_1, \boldsymbol{F}\boldsymbol{\kappa}_2)_2 = \boldsymbol{\kappa}_2^H \boldsymbol{F}^H \boldsymbol{F} \boldsymbol{\kappa}_1 = \boldsymbol{\kappa}_2^H \boldsymbol{M} \boldsymbol{\kappa}_1 = (\boldsymbol{q}_1, \boldsymbol{q}_2)_{\mathscr{M}}$$

and its associated vector norm satisfies

$$\|\boldsymbol{\kappa}\|_{\boldsymbol{M}} = \|\boldsymbol{F}\boldsymbol{\kappa}\|_2 = \|\boldsymbol{q}\|_{\mathscr{M}}, \quad \boldsymbol{q} \in \mathscr{S}^N.$$

For matrices $\boldsymbol{B} \in \mathscr{C}^{N \times N}$, the energy norm is defined in terms of the vector norm in the standard manner.

In what follows we will, if not otherwise stated, use the discrete scalar product and norm based on the energy density and will, therefore, omit the subscript $\boldsymbol{M}$ hereafter.

2.3. *Transient growth and pseudospectra*

It is a key issue of this work to generally distinguish two temporal domains in the analysis of linear stability. The two domains demand different tools to investigate stability. In one domain we are concerned with the asymptotic stability in the limit of large time, whereas in the other domain we will focus our attention on the short-time behaviour of solutions to the underlying initial value problem.

In order to illustrate this issue, it is most instructive to consider the formal solution of the initial value problem (7), which can be written as

$$\boldsymbol{\kappa} = \exp(-\mathrm{i}\tau\boldsymbol{\Lambda})\boldsymbol{\kappa}_0, \quad \boldsymbol{\kappa}_0 = \boldsymbol{\kappa}(\tau = 0).$$

The maximum possible amplification G of initial energy density is given by

$$G(\tau) = \sup_{\kappa_0 \neq 0} \frac{\|\boldsymbol{\kappa}\|^2}{\|\boldsymbol{\kappa}_0\|^2} = \|\exp(-\mathrm{i}\tau\boldsymbol{\Lambda})\|^2 = \|\boldsymbol{F}\exp(-\mathrm{i}\tau\boldsymbol{\Lambda})\boldsymbol{F}^{-1}\|_2^2. \tag{8}$$

To further our insight, upper and lower bounds on the norm of the matrix exponential are given as follows:

$$\exp(\omega_i\tau) \leqslant \|\exp(-\mathrm{i}\tau\boldsymbol{\Lambda})\| \leqslant \|\boldsymbol{F}\|_2 \|\boldsymbol{F}^{-1}\|_2 \exp(\omega_i\tau) = \kappa(\boldsymbol{F})\exp(\omega_i\tau),$$

where ω_i denotes the imaginary part of the least stable eigenvalue of $\boldsymbol{\Lambda}$ and the quantity $\kappa(\boldsymbol{F}) = \|\boldsymbol{F}\|_2 \|\boldsymbol{F}^{-1}\|_2$ is known as the condition number of the matrix $\boldsymbol{F}$ and is greater than or equal to one.

Two cases have to be distinguished.

If $\kappa(\boldsymbol{F})$ equals one, the upper and lower bounds coincide and the temporal evolution of the maximum amplification factor G is dictated by the least-stable eigenvalue for all times.

If $\kappa(\boldsymbol{F})$ is substantially larger than one, then the behaviour of $G(\tau)$ is determined by ω_i only in the asymptotic limit of large times. For short times, there may be substantial transient growth although $\omega_i < 0$.

Recall that the matrix $\boldsymbol{\Lambda}$ represents the evolution operator $\mathscr{L}_1$ projected onto the space $\mathscr{S}^N$. $\mathscr{L}_1$ is called normal if it commutes with its adjoint, i.e. $\mathscr{L}_1 \mathscr{L}_1^+ = \mathscr{L}_1^+ \mathscr{L}_1$, where the adjoint is defined by the relation $(\mathscr{L}_1 \boldsymbol{q}, \boldsymbol{q})_{\mathscr{M}} = (\boldsymbol{q}, \mathscr{L}_1^+ \boldsymbol{q})_{\mathscr{M}}$. A necessary and sufficient condition for an operator to be normal is that it has orthogonal eigenfunctions (Kato 1976), i.e. $(\tilde{\boldsymbol{q}}_i, \tilde{\boldsymbol{q}}_j)_{\mathscr{M}} = \delta_{ij}$. In terms of the projection onto $\mathscr{S}^N$ this implies $\kappa(\boldsymbol{F}) = 1$ if $\mathscr{L}_1$ is normal and $\kappa(\boldsymbol{F}) > 1$ if $\mathscr{L}_1$ is non-normal. Note that the adjoint of $\boldsymbol{\Lambda}$ in $\mathscr{S}^N$ is $\boldsymbol{\Lambda}^+ = \boldsymbol{M}^{-1}\boldsymbol{\Lambda}^H\boldsymbol{M}$, implying that $\boldsymbol{\Lambda}^+\boldsymbol{\Lambda} = \boldsymbol{\Lambda}\boldsymbol{\Lambda}^+$ if $\boldsymbol{M} = \boldsymbol{I}$.

The linear evolution operator for infinitesimal disturbances in circular pipe flow is of non-normal type, thus limiting the information content of the spectrum to the behaviour for large times. In order to also capture short-time transient behaviour of non-normal operators, a generalization of the concept of spectra based on the resolvent norm of the linear operator can be defined.

This leads to the definition of ϵ-pseudospectra, introduced by Trefethen (1992) to analyse the behaviour of non-normal operators and matrices. A number $z \in \mathscr{C}$ lies in the ϵ-pseudospectrum of a matrix $\boldsymbol{A}$, which we denote by $\boldsymbol{\Lambda}_\epsilon(\boldsymbol{A})$, if either of the following equivalent conditions is satisfied:

DEFINITION 1. z is an eigenvalue of $\tilde{\boldsymbol{A}} = \boldsymbol{A} + \boldsymbol{E}$ for some perturbation matrix $\boldsymbol{E}$ with $\|\boldsymbol{E}\| \leqslant \epsilon$;

DEFINITION 2. $z \in \mathscr{C}$ and $\|(z\boldsymbol{I} - \boldsymbol{A})^{-1}\| \geqslant \epsilon^{-1}$.

The definitions for operators are essentially the same. For the details, see Reddy *et al.* (1993).

The first definition relates the ϵ-pseudospectrum to the spectrum of a randomly perturbed matrix: z is considered an ϵ-pseudoeigenvalue of $\boldsymbol{A}$ if it is an exact eigenvalue of a matrix $\tilde{\boldsymbol{A}}$ which is perturbed by a random matrix $\boldsymbol{E}$ of norm ϵ.

The second definition uses the norm of the resolvent $\boldsymbol{R}(z) = (z\boldsymbol{I} - \boldsymbol{A})^{-1}$, which is continuously defined in the complex plane with the exception of the spectrum of $\boldsymbol{A}$. The point spectrum of $\boldsymbol{A}$ will correspond to the locations where the norm of the resolvent tends to infinity. For finite but large resolvent norm, z will be defined as an ϵ-pseudo-eigenvalue of $\boldsymbol{A}$ with $\epsilon = 1/\|\boldsymbol{R}(z)\|$.

For our case, the norm of the resolvent is most easily calculated by the singular value decomposition as

$$\|(z\boldsymbol{I} - \boldsymbol{\Lambda})^{-1}\| = \left\| \boldsymbol{F} \operatorname{diag}\left(\frac{1}{z-\omega_1}, \ldots, \frac{1}{z-\omega_N} \right) \boldsymbol{F}^{-1} \right\|_2$$

$$= \sigma_1 \left(\boldsymbol{F} \operatorname{diag}\left(\frac{1}{z-\omega_1}, \ldots, \frac{1}{z-\omega_N} \right) \boldsymbol{F}^{-1} \right),$$

where σ_1 denotes the largest singular value.

It is important to note that both definitions describe the ϵ-pseudospectrum as a parameter-dependent *region* in the complex plane rather than a discrete set.

A link between the occurrence of transient growth and the ϵ-pseudospectrum is given by the Hille–Yosida theorem (Kato 1976; Pazy 1983), which states that the energy amplification G maximized over time and denoted by G_{max} is equal to one (which is equivalent to no transient growth) if and only if the quantity

$$\gamma_\epsilon \equiv \sup_{\epsilon \geqslant 0} \frac{\beta(\epsilon)}{\epsilon} \tag{9}$$

is less than one, where $\beta(\epsilon)$ is the maximum imaginary part of the ϵ-pseudospectrum in the unstable half-plane. An application given in §3 will illustrate the use of this theorem. This means that growth can be estimated from the quantity γ_ϵ that measures how far the pseudospectrum reaches into the unstable half-plane. Not only does the quantity γ_ϵ give information about the potential for transient growth, it also provides a lower bound for the maximum possible growth G_{max} as the following inequality holds (Trefethen 1992):

$$G_{max} \geqslant \gamma_\epsilon^2.$$

An upper bound for the maximum growth G_{max} can be derived from the ϵ-pseudospectrum via resolvent integrals. For further details the reader is referred to Reddy *et al.* (1993).

2.4. *Optimal disturbances*

It is important to keep in mind that the curve given by $\|\exp(-\mathrm{i}\tau\boldsymbol{\Lambda})\|$ represents the maximum possible energy amplification, which for each instant of time is optimized over all possible initial conditions with unit energy norm. The initial condition that optimizes the amplification factor might be different for different times, so that $\|\exp(-\mathrm{i}\tau\boldsymbol{\Lambda})\|$ should be thought of as the envelope of the energy evolution of individual initial conditions with unit energy norm.

However, it is not difficult to determine the initial condition that will reach the maximum possible amplification at a given time τ_0 and will be tangent to $\|\exp(-\mathrm{i}\tau\boldsymbol{\Lambda})\|$ at τ_0. The procedure is best understood in terms of the singular value decomposition (SVD). Let us deompose the matrix $\boldsymbol{B} = \boldsymbol{F}\exp(-\mathrm{i}\tau_0\boldsymbol{\Lambda})\boldsymbol{F}^{-1}$ according to

$$\boldsymbol{B}\boldsymbol{V} = \boldsymbol{U}\boldsymbol{\Sigma},$$

where $\boldsymbol{V}$ and $\boldsymbol{U}$ are unitary matrices and $\boldsymbol{\Sigma}$ is a diagonal matrix consisting of the singular values, $\boldsymbol{\Sigma} = \mathrm{diag}\{\sigma_1, \ldots, \sigma_N\}$, $\sigma_j \in \mathscr{R}_0^+$ which are ordered in size, i.e. $\sigma_1 \geqslant \sigma_2 \geqslant \ldots \geqslant \sigma_N$.

The 2-norm of $\boldsymbol{B}$, equivalent to the energy norm of $\exp(-\mathrm{i}\tau\boldsymbol{\Lambda})$, is given by the largest singular value σ_1. Concentrating only on the column vectors of $\boldsymbol{V}$ and $\boldsymbol{U}$ corresponding to σ_1, which are referred to as the principal right and left singular vectors, respectively, one obtains

$$\boldsymbol{B}\boldsymbol{v}_1 = \sigma_1\boldsymbol{u}_1.$$

This describes a mapping $\boldsymbol{B}$ of an input vector $\boldsymbol{v}_1$ onto an output vector $\boldsymbol{u}_1$ which is in addition stretched by a factor of σ_1 equal to the 2-norm of $\boldsymbol{B}$. Therefore, $\boldsymbol{v}_1$ describes the initial condition that will be amplified by a factor of $\sigma_1 = \|\boldsymbol{B}\|_2$ due to the mapping $\boldsymbol{F}\exp(-\mathrm{i}\tau_0\boldsymbol{\Lambda})\boldsymbol{F}^{-1}$. Here τ_0 is the time at which this amplification will be reached. In order to extract the coefficients κ_1 of the initial condition we have to express $\boldsymbol{v}_1$ in the basis $\{\tilde{\boldsymbol{q}}_1, \ldots, \tilde{\boldsymbol{q}}_N\}$, which is accomplished by

$$\boldsymbol{\kappa}_1 = \boldsymbol{F}^{-1}\boldsymbol{v}_1. \tag{10}$$

In short, the coefficients for the disturbance that will reach its maximum possible amplification at a given time τ_0 are given by (10), where v_1 stands for the principal right singular vector of the matrix $\boldsymbol{F}\exp(-\mathrm{i}\tau_0\boldsymbol{\Lambda})\boldsymbol{F}^{-1}$. An alternative method to compute the optimal disturbances is using the calculus of variations (see Butler & Farrell 1992).

It should be noted that the initial condition κ_1 may reach higher energies after τ_0, but at the time τ_0, it will be the unique initial disturbance among all unit energy initial disturbances that will reach the maximum possible energy amplification. The phrase 'maximum possible amplification at τ_0' is thus an optimization over initial conditions with unit energy norm, rather than an optimization over time.

With this note, we conclude the theoretical background on the tools to study linear stability of bounded shear flows and will now consider applications to the stability of incompressible viscous flow in a circular pipe.

2.5. *Energy equations and the numerical range*

Up to this point only perturbations of infinitesimal amplitudes have been considered. A different approach to hydrodynamic stability theory is concerned with the calculation of critical Reynolds numbers below which disturbances of arbitrary amplitude will experience monotonic decay. This approach, which is known as the energy or absolute stability method (Joseph & Carmi 1969), is based on the evolution equation for the perturbation energy, which is referred to as the Reynolds–Orr equation (see e.g. Drazin & Reid 1981).

In order to put the analysis of this section into perspective, we will briefly digress to elaborate on the derivation and implications of the Reynolds–Orr equation, which is most conveniently done in terms of vector calculus for primitive variables. The equation of motion for the disturbance velocity $\boldsymbol{u}$ about a steady mean state $\boldsymbol{U}$ reads

$$\left.\begin{aligned} \frac{\partial}{\partial t}\boldsymbol{u}+(\boldsymbol{u}\cdot\boldsymbol{\nabla})\,\boldsymbol{U}+(\boldsymbol{U}\cdot\boldsymbol{\nabla})\,\boldsymbol{u}+(\boldsymbol{u}\cdot\boldsymbol{\nabla})\,\boldsymbol{u} &= -\boldsymbol{\nabla}p-\frac{1}{R}(\boldsymbol{\nabla}\times\boldsymbol{\nabla}\times\boldsymbol{u}),\\ \boldsymbol{\nabla}\cdot\boldsymbol{u} &= 0. \end{aligned}\right\} \tag{11}$$

To arrive at the evolution equation for the total disturbance energy, defined as

$$\mathscr{E}=\frac{1}{2}\int|\boldsymbol{u}|^2\,\mathrm{d}\boldsymbol{x},$$

where the integral is taken over the entire domain under consideration, we take the scalar product of (11) and $\boldsymbol{u}$, and integrate the resulting expression. We obtain

$$\begin{aligned} \frac{\mathrm{d}}{\mathrm{d}t}\mathscr{E} &= -\int\left((\boldsymbol{u}\cdot\boldsymbol{\nabla})\,\boldsymbol{U}\cdot\boldsymbol{u}+\frac{1}{R}|\boldsymbol{\nabla}\boldsymbol{u}|^2\right)\mathrm{d}\boldsymbol{x}-\int\boldsymbol{\nabla}\cdot(\tfrac{1}{2}(\boldsymbol{U}+\boldsymbol{u})\,|\boldsymbol{u}|^2+\boldsymbol{u}p)\,\mathrm{d}\boldsymbol{x}\\ &= -\int\left((\boldsymbol{u}\cdot\boldsymbol{\nabla})\,\boldsymbol{U}\cdot\boldsymbol{u}+\frac{1}{R}|\boldsymbol{\nabla}\boldsymbol{u}|^2\right)\mathrm{d}\boldsymbol{x}-\int\tfrac{1}{2}((\boldsymbol{U}+\boldsymbol{u})\,|\boldsymbol{u}|^2+\boldsymbol{u}p)\,\mathrm{d}\boldsymbol{S}, \end{aligned}$$

where the vector identity $\boldsymbol{u}\cdot((\boldsymbol{U}\cdot\boldsymbol{\nabla})\,\boldsymbol{u}+(\boldsymbol{u}\cdot\boldsymbol{\nabla})\,\boldsymbol{u}+\boldsymbol{\nabla}p)=\boldsymbol{\nabla}\cdot(\frac{1}{2}(\boldsymbol{U}+\boldsymbol{u})\,|\boldsymbol{u}|^2+\boldsymbol{u}p)$ valid for solenoidal $\boldsymbol{u}$ and $\boldsymbol{U}$, as well as the divergence theorem have been employed. The integral over the boundary S of the fluid domain will vanish for spatially periodic or localized disturbances. As we will only be concerned with spatially periodic disturbances, we can further simplify the equation above, to arrive at

$$\frac{\mathrm{d}}{\mathrm{d}t}\mathscr{E}=-\int(\boldsymbol{u}\cdot\boldsymbol{\nabla})\,\boldsymbol{U}\cdot\boldsymbol{u}\,\mathrm{d}\boldsymbol{x}-\frac{1}{R}\int|\boldsymbol{\nabla}\boldsymbol{u}|^2\,\mathrm{d}\boldsymbol{x}. \tag{12}$$

This equation is the starting point for determining the critical Reynolds number below which the energy of a general finite-amplitude disturbance will decay. For details on the solution procedure, which rests upon the calculus of variations, the interested reader is directed to Joseph & Carmi (1969).

It is important to notice that the nonlinear terms of (11), i.e. $(\boldsymbol{u}\cdot\boldsymbol{\nabla})\boldsymbol{u}$, do not enter the Reynolds–Orr equation (12). Thus, any gain in total disturbance energy has to stem from a linear process, which according to (12) can be described as a balance of mean flow interaction and viscous dissipation.

This essential result will now motivate the use of the linearized initial value problem (7) in the derivation of the evolution equation for the energy norm in terms of the notation introduced in (6).

It follows from the definition of the scalar product and its associated norm that

$$\frac{\partial}{\partial\tau}\|\boldsymbol{\kappa}\|^2 = \left(\frac{\partial\boldsymbol{\kappa}}{\partial\tau},\boldsymbol{\kappa}\right)+\left(\boldsymbol{\kappa},\frac{\partial\boldsymbol{\kappa}}{\partial\tau}\right) = (-\mathrm{i}\boldsymbol{\Lambda}\boldsymbol{\kappa},\boldsymbol{\kappa})+(\boldsymbol{\kappa},-\mathrm{i}\boldsymbol{\Lambda}\boldsymbol{\kappa}) = 2\,\mathrm{Im}\,(\boldsymbol{\Lambda}\boldsymbol{\kappa},\boldsymbol{\kappa}). \tag{13}$$

The equation governing the total perturbation energy is obtained by summing (13) over all streamwise and azimuthal wavenumbers:

$$\frac{\partial}{\partial\tau}\mathscr{E} = \frac{1}{4\pi^2}\sum_{m,n}\frac{\partial}{\partial\tau}\|\boldsymbol{\kappa}_{mn}\|^2 = \frac{1}{2\pi^2}\sum_{m,n}\mathrm{Im}\,(\boldsymbol{\Lambda}_{mn}\boldsymbol{\kappa}_{mn},\boldsymbol{\kappa}_{mn}),$$

where $\boldsymbol{\kappa}_{mn}$ is the vector of eigenfunction expansion coefficients for the streamwise wavenumber $\alpha_m = m\alpha$ and azimuthal wavenumber n. This equation is identical to (12) because the nonlinear terms of (11) do not contribute to the temporal evolution of the total perturbation energy. The sign of the imaginary part of $(\boldsymbol{\Lambda}\boldsymbol{\kappa},\boldsymbol{\kappa})$ determines whether the rate of change of energy density $\|\boldsymbol{\kappa}\|^2$ is positive or negative, as can easily be seen from (13).

Using the adjoint we can rewrite (13) as

$$\frac{\partial}{\partial\tau}\|\boldsymbol{\kappa}\|^2 = 2\,\mathrm{Im}\{(\boldsymbol{\Lambda}\boldsymbol{\kappa},\boldsymbol{\kappa})\} = \|\boldsymbol{L}\boldsymbol{\kappa}\|^2,$$

where $\boldsymbol{L}^H\boldsymbol{L} = -\mathrm{i}(\boldsymbol{\Lambda}-\boldsymbol{\Lambda}^+)$. Thus, the maximum growth rate possible can be determined as

$$\max_{\|\boldsymbol{\kappa}\|=1}\|\boldsymbol{L}\boldsymbol{\kappa}\|^2 = \|\boldsymbol{L}\|^2.$$

The quantity $(\boldsymbol{\Lambda}\boldsymbol{\kappa},\boldsymbol{\kappa})$ defines the numerical range in the following manner.

$$\mathscr{F}(\boldsymbol{\Lambda}) = \{z\colon z = (\boldsymbol{\Lambda}\boldsymbol{\kappa},\boldsymbol{\kappa}),\quad \|\boldsymbol{\kappa}\| = 1\}.$$

Thus the maximum of the imaginary part of the numerical range of $\boldsymbol{\Lambda}$ determines the growth rate in energy density for $\tau = 0^+$ exactly, as can be easily demonstrated with an expansion around $t = 0$.

It follows that the condition for energy density growth can be restated in terms of the numerical range: a necessary and sufficient condition for the growth of energy density is that the numerical range $\mathscr{F}(\boldsymbol{\Lambda})$ extends into the upper complex half-plane. Thus, the critical Reynolds number below which no energy density growth is possible is equivalent to the Reynolds number for which the numerical range is entirely confined to the stable half-plane with the boundary of the numerical range tangent to the real axis. This critical Reynolds number thus coincides with the one obtained by the energy

stability method (Joseph & Carmi 1969) which is based on a variational principle applied to (12). This has been discussed by Reddy & Henningson (1993) and Henningson & Reddy (1994).

The numerical range can be calculated using standard techniques which can be found in, for example, Horn & Johnson (1991).

3. Numerical results

In this section we will apply the tools developed in the previous section to investigate the linear stability of solutions to the initial value problem (7). Before launching into this analysis, we shall briefly describe the numerical method used throughout this presentation.

A hybrid spectral collocation technique (see Herbert 1977) based on Chebyshev polynomials is employed to spatially discretize the initial-boundary-value problem. A linear mapping of the radial coordinate $r \in [0, 1]$ onto the interval $\xi \in [-1, 1]$ has been chosen, which results in an expansion of the flow quantities of the form

$$\hat{\Phi}(r) = \sum_{k=0}^{K} \hat{\Phi}_k T_k(2r-1), \qquad \hat{\Omega}(r) = \sum_{k=0}^{K} \hat{\Omega}_k T_k(2r-1).$$

The Chebyshev polynomials are evaluated at the Gauss–Lobatto collocation points given as

$$\xi_j = 2r_j - 1 = \cos(j\pi/K), \quad j = 0, 1, \ldots, K,$$

where $K+1$ is both the maximum number of collocation points and the number of Chebyshev polynomials. The resulting spatially discretized equations are solved for the unknown expansion coefficients $(\hat{\Phi}_k\ \hat{\Omega}_k)$ with $k = 0, \ldots, K$.

Coordinate singularities at the centre of the pipe are avoided by imposing boundary conditions at the matrix rows corresponding to the collocation points at $r = 0$ instead of solving the governing equations at this collocation point.

3.1. *Asymptotic behaviour*

Linear stability is concerned with the evolution of disturbances of infinitesimal amplitude in the asymptotic limit of large times. To this end, the temporal behaviour of the disturbances is assumed to be of the form $\exp(-i\omega\tau)$, with ω the complex frequency. If the imaginary part of ω is positive, the mean flow field is said to be linearly unstable; if the imaginary part of ω is negative, it is linearly stable. A perturbation with vanishing imaginary part of ω defines the mean field as neutrally stable.

Mathematically, the assumption of mode-like temporal behaviour transforms the initial-boundary-value problem (1) into a generalized eigenvalue problem (5). In all cases presented, the generalized problem has been reduced to a standard eigenvalue problem which was then solved by the QR-algorithm.

Figure 1 shows the pipe flow spectrum Λ_R for the parameters $\alpha = 1$, $n = 1$ and $R = 3000$. Sixty Chebyshev polynomials have been used to accurately represent radial velocity and radial vorticity. The spectrum shows the typical three-branch structure similar to spectra for plane Poiseuille or Couette flow (Drazin & Reid 1981), allowing an analogous classification of eigensolutions into so-called wall modes, centre modes and mean modes. Wall modes are characterized by a vanishing phase velocity $c_r = \mathrm{Re}(\omega/\alpha R)$ as the product of streamwise wavenumber and Reynolds number increases; centre modes on the other hand propagate at almost the pipe centreline velocity for

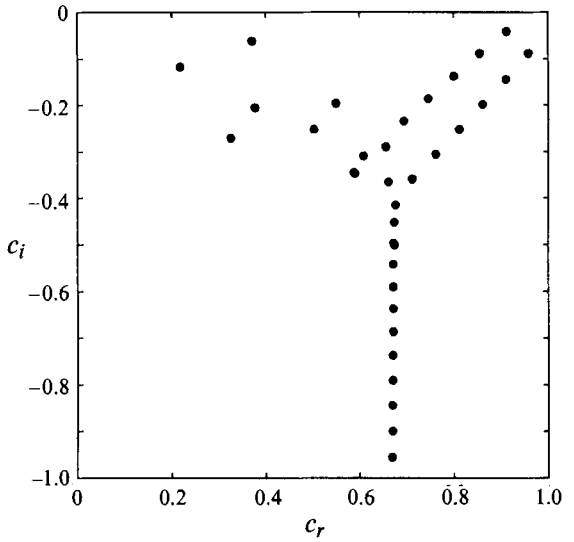

FIGURE 1. Pipe flow spectrum Λ_R for $\alpha = 1$, $n = 1$, $R = 3000$. $N = 60$ Chebyshev polynomials have been used to discretize the normal direction.

large αR, and mean modes are characterized by a phase velocity of $\frac{2}{3}$ as αR tends to zero (Drazin & Reid 1981):

$$\text{wall modes:} \quad c_r \to 0 \quad \text{as} \quad \alpha R \to \infty;$$

$$\text{centre modes:} \quad c_r \to 1 \quad \text{as} \quad \alpha R \to \infty;$$

$$\text{mean modes:} \quad c_r \to \tfrac{2}{3} \quad \text{as} \quad \alpha R \to 0.$$

It is interesting to note that for increasing Reynolds numbers R, the number of wall modes monotonically decreases (Metcalfe & Orszag 1973; Salwen *et al.* 1980).

Two distinct special cases follow from the general equations.

(i) For $n = 0$, the governing equations describe the evolution of axisymmetric perturbations. Axisymmetric disturbances are entirely determined by the radial velocity component, as the streamwise velocity follows from the continuity equation. The radial vorticity for axisymmetric disturbances is zero.

(ii) For $\alpha = 0$, the governing equations reduce to the evolution equations for two-dimensional disturbances. For this case, the viscous off-diagonal coupling terms vanish, which allows one to separate the vector eigenfunctions into radial velocity and radial vorticity modes. However, the inviscid coupling term, forcing the radial vorticity equation, persists even for two-dimensional perturbations, which results in a particular radial vorticity component associated with each radial velocity mode.

For three-dimensional and non-axisymmetric disturbances, the eigensolutions of the vector equation cannot uniquely be separated into velocity and vorticity modes, but rather have to be viewed as a compound quantity.

Two types of errors have to be distinguished when accurately calculating the eigenvalues: truncation error and roundoff error. Although both types of error ultimately result in erroneous eigenvalues, their effect on the spectrum has a quite distinct character. Truncation error is due to insufficient resolution and will especially affect higher mean modes. This is because these modes show increasingly oscillatory behaviour in both the real and imaginary parts, which a low number of expansion

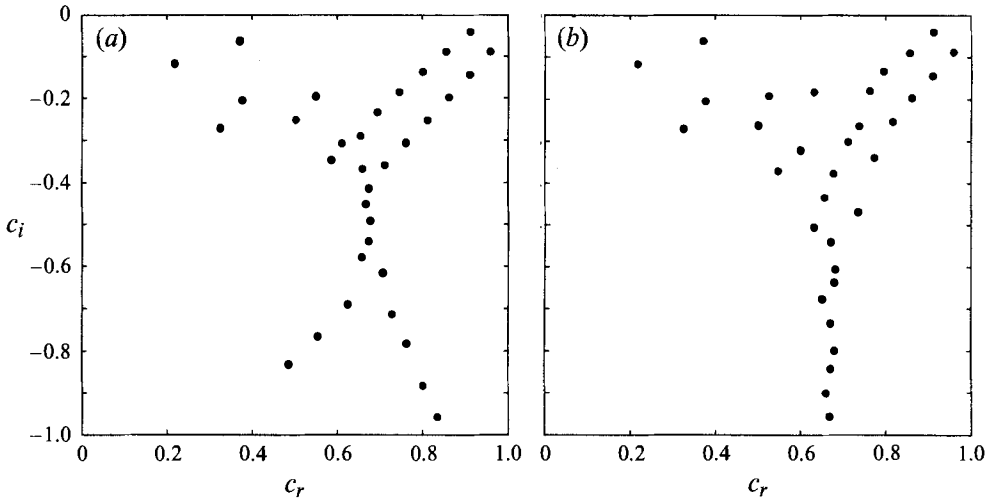

FIGURE 2. Pipe flow spectrum Λ_R for $\alpha = 1$, $n = 1$, $R = 3000$. (*a*) Effect of truncation; $N = 32$ Chebyshev polynomials have been used in the normal direction. (*b*) Effect of roundoff (16 bits have been used).

functions fails to approximate properly. Roundoff errors, on the other hand, are due to the finite representation of floating point numbers on a digital computer and cannot be controlled by an increase in the number of basis functions. Particularly for high Reynolds numbers, roundoff error is found to have a considerable impact on the eigenvalues in the intersection of the eigenvalue branches.

Figure 2(*a*) shows the pipe flow spectrum for the same values as chosen for figure 1, but only 32 Chebyshev polynomials have been used to discretize the radial direction. A characteristic splitting of the mean-mode branch is observed which has also been found by Davey & Drazin (1969), but has not been associated with a lack of resolution.

Figure 2(*b*) illustrates the effect of roundoff errors on the spectrum. Calculations have been performed using a lower number of bits to represent floating point numbers, thus artificially increasing machine roundoff. The eigenvalues close to the region where the three eigenvalue branches intersect are especially affected and can deviate by orders of magnitude more than the perturbation imposed on them. This issue is related to the ϵ-pseudoeigenvalues according to definition 1 and will be addressed in more detail in the next section.

As the literature on linear pipe flow stability for three-dimensional non-axisymmetric disturbances has not included modes with higher damping rates, we will list the least stable eigenvalues of Λ_R for some selected parameter combinations (see table 1). Owing to the effect of truncation and roundoff error on the accuracy of the eigenvalues as described above, only digits are listed that were invariant both to a reduction in the number of Chebyshev polynomials and to a reduction in the number of bits to represent floating point numbers. As a general trend, fewer significant digits are observed for eigenvalues near the intersection of the three eigenvalue branches. All calculations have been carried out on a CRAY-XMP in single precision (16 bits) and good agreement up to the accuracy of previously published results (Metcalfe & Orszag 1973; Salwen *et al.* 1980) has been found.

$n = 0$		$n = 1$		$n = 2$		$n = 3$	
Real	Imaginary	Real	Imaginary	Real	Imaginary	Real	Imaginary
0.94836022	−0.05197311	0.91146557	−0.04127564	0.888297659	−0.06028569	0.86436392	−0.08325398
0.948360198	−0.051973123	0.3709351	−0.06161902	0.352554927	−0.08789898	0.34640195	−0.105708407
0.896719201	−0.103612364	0.958205543	−0.08834603	0.83289336	−0.10883834	0.214919870	−0.116877921
0.8967204	−0.1036129	0.8547888	−0.0888702	0.939497220	−0.112001616	0.809746802	−0.13239243
0.412396334	−0.112217160	0.216803863	−0.1168771536	0.2154918165	−0.115514380	0.916719175	−0.13603546
0.21843581	−0.121310028	0.799699	−0.1374903	0.77858499	−0.15810861	0.7558793	−0.1820364
0.84507180	−0.15522017	0.9100373	−0.1443461	0.890618 5726	−0.16729405	0.867413655	−0.190639837
0.8450807	−0.155253	0.745304	−0.186433	0.72507714	−0.2075915	0.37123650	−0.212779412
0.3762424	−0.2004630	0.549312	−0.195839	0.37502654	−0.209314329 99	0.7030072	−0.231818
0.793784 13	−0.20647681	0.86074946	−0.1986461	0.84097538	−0.221474731	0.5517316	−0.244111
0.793441	−0.2068929	0.37643141	−0.20495551	0.5516823	−0.2282286	0.81757000	−0.2444956
0.626297 00	−0.22746562	0.693462	−0.23433	0.50087191	−0.2498031	0.4992922	−0.2511428
0.502037	−0.257316	0.5026425	−0.2518091	0.6752208	−0.257968	0.3614494797	−0.26190688
0.741758	−0.258508	0.810845	−0.2521235	0.342097 17	−0.263 13898	0.655473	−0.285153
0.7470465	−0.2588806	0.325 13026	−0.270458 58	0.790895 11	−0.27503702	0.7674456	−0.2978449
0.347 39229	−0.297526503	0.65506	−0.289647	0.602773	−0.308898	0.597828	−0.307366
0.61086	−0.301052	0.760702	−0.305127	0.7409255	−0.328 1990	0.623701	−0.346886
0.69261	−0.308166	0.60793	−0.309010	0.640087	−0.3321112	0.718097	−0.350987
0.7103043	−0.324318	0.587438	−0.3447905	0.614160	−0.3430168	0.652416	−0.376204
0.67458	−0.324318	0.711237	−0.35914	0.692965	−0.382998	0.677885	−0.411035
0.6004525	−0.3814682	0.660391	−0.365684	0.6664413	−0.4059762	0.668061	−0.4492620
0.6823494	−0.406651	0.67587	−0.414687	0.673136	−0.4537154	0.670477	−0.496004
0.672883	−0.453187	0.673368	−0.451428	0.6707368	−0.4948720	0.66818287	−0.5386278
0.6736237	−0.496799	0.671987	−0.497340	0.6708278	−0.5419932	0.6694102	−0.5875345
0.671515	−0.542212	0.671460	−0.541600	0.6696647	−0.586958 54	0.6673482	−0.63326489
0.6717237	−0.588886	0.670781	−0.588958	0.6699829	−0.636547 11	0.6689383	−0.6848609
0.670474	−0.636976	0.6703508	−0.636355	0.668767911	−0.6845895	0.66667638	−0.7338322
0.6708160	−0.6864667	0.6699896	−0.686604	0.6694481	−0.7370286	0.668645268	−0.788 16043
0.669683	−0.737636	0.669 54242	−0.7369640	0.668079 50	−0.788211 14	0.666183895	−0.840490 90
0.670 15960	−0.7899999	0.6694100	−0.7902089	0.669 06443	−0.8435236	0.6684402	−0.897552 14
0.669078	−0.844317	0.6689184	−0.8436119	0.667 55609	−0.897947 50	0.665834 66	−0.953322 78
0.6696446	−0.8996122	0.6689736	−0.8998743	0.6687743	−0.956 13894		
0.668611	−0.957120	0.6684327	−0.956400 32				

TABLE 1. Eigenvalues for $\alpha = 1$, $R = 3000$ and three selected values of the azimuthal wavenumber n

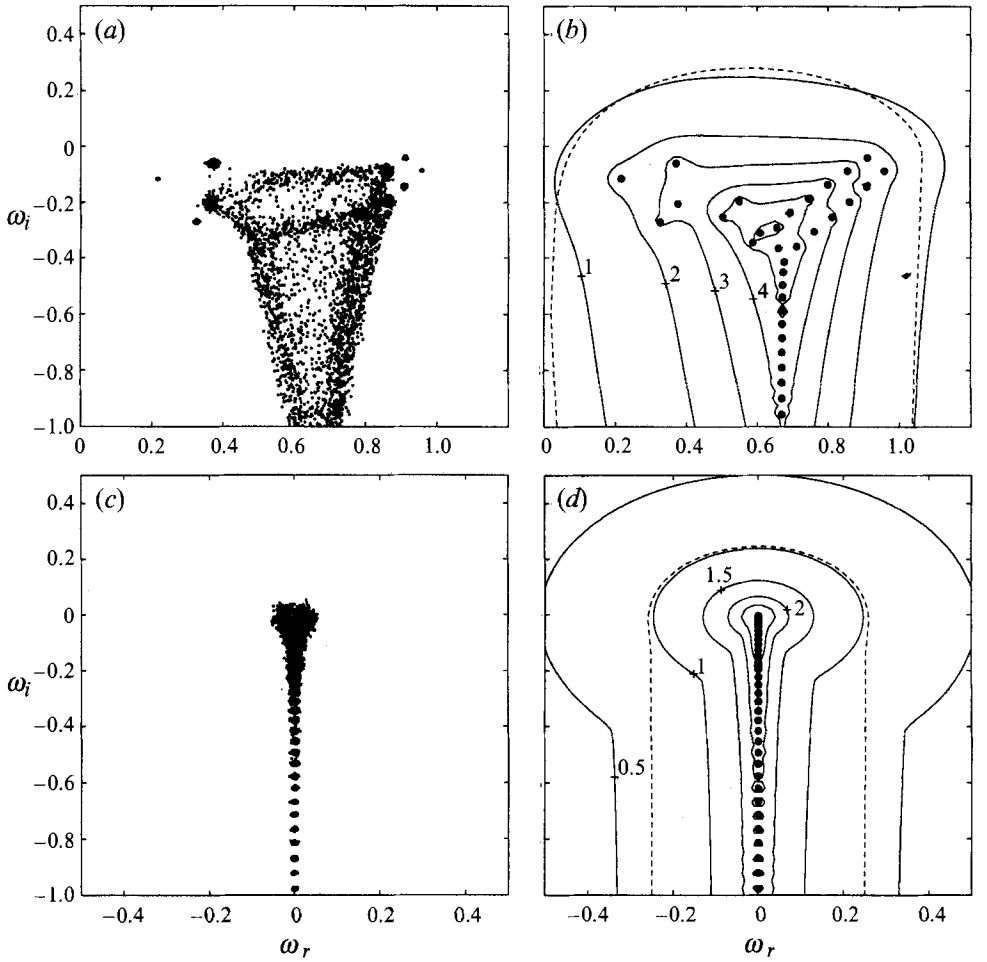

FIGURE 3. Pseudospectrum of A_R for circular pipe flow. (*a*) $\alpha = 1$, $n = 1$, $R = 3000$, superposition of 100 spectra of the matrix A_R perturbed by matrices of energy norm 10^{-3}. (*b*) Same parameters as in (*a*), contours of constant resolvent norm. (*c*) $\alpha = 0$, $n = 1$, $R = 3000$, superposition of 100 spectra of the matrix A_R perturbed by matrices of energy norm 10^{-2}. (*d*) Same parameters as in (*c*), contours of constant resolvent norm. The numbers on the contours specify the base-10 logarithm of the resolvent norm, i.e. a (closed) contour labelled 2 contains points at whose location the resolvent is larger than 10^2. Equivalently, perturbations on the matrix A_R of norm 10^{-2} would be confined to the region in the complex plane encircled by the contours labelled 2. The dashed line in (*b*) and (*d*) represents the boundary of the numerical range of A_R.

3.2. *Pseudospectra, sensitivity and the numerical range*

It is important to stress again that linear theory based on eigenvalues generally explores the stability of a flow field in an asymptotic setting for large times. Only for normal operators, i.e. operators that have *orthogonal* eigenfunctions, are eigenvalues sufficient to describe the temporal behaviour for all times. The stability operator for circular pipe flow is of non-normal type and in this section we will examine the occurrence of transient effects where use will be made of the tools developed earlier.

Following the first definition of ϵ-pseudo-eigenvalues, figure 3(*a*) shows a superposition of 100 spectra of the evolution matrix for $\alpha = 1$, $n = 1$ and $R = 3000$ perturbed by random matrices of norm 10^{-3}. It is observed that a perturbation of norm

10^{-3} can cause some eigenvalues to shift by a distance of order one. This sensitivity is highest for eigenvalues at the intersection point of the three eigenvalue branches, which also confirms the effect of roundoff error depicted in figure 2(*b*). Figure 3(*b*), displaying the resolvent-norm contours together with the unperturbed spectrum, gives the complete picture of the ϵ-pseudospectrum of the stability matrix for the specified parameter values.

Figures 3(*c*) and 3(*d*) display the ϵ-pseudospectrum for the case of two-dimensional disturbances, i.e. with $\alpha = 0$. The spectrum is markedly different, showing purely imaginary eigenvalues for which analytical expressions exist (Bergström 1992). It is evident from the ϵ-pseudospectrum for this case that small perturbations can result in eigenvalues in the unstable half-plane. This is also illustrated by the resolvent-norm contours (figure 3*d*), which extend into the unstable half-plane even for moderate contour levels.

It can be seen that in cases of both zero and non-zero streamwise wavenumber even a minute perturbation can have an appreciable effect on the location of the eigenvalues in certain regions of the spectrum.

An even more important implication of non-normality is the potential for transient growth in energy density. Recalling inequality (9), the ϵ-pseudospectrum depicted in figure 3(*d*) enables us to give a lower estimate for the expected transient growth maximum. The contour labelled 2, for example, reaches a distance of about 0.07 into the upper half-plane. Therefore, we anticipate the maximum G_{max} of the transient growth curve to be larger than $(0.07/10^{-2})^2 = 49$. Other contour values may give better estimates for the maximum. A similar estimate for G_{max} can be determined for $\alpha = 1$ from figure 3(*b*).

As has been stated in §2.5, the numerical range of Λ_R, whose boundary is displayed by the dashed line in figures 3(*b*) and 3(*d*), determines the growth rate of the energy density for $t = 0^+$. For both parameter combinations chosen, the numerical range extends into the unstable half-plane. In the case of three-dimensional perturbations ($\alpha = 1$) a maximum initial energy density growth rate

$$\frac{\mathrm{d}\|\boldsymbol{\kappa}\|^2}{\mathrm{d}t}\Big|_{t=0} = 2 \max \mathrm{Im}\,(\Lambda_R \boldsymbol{\kappa}, \boldsymbol{\kappa})$$

of 0.5629 is expected; for two-dimensional disturbances ($\alpha = 0$) the maximum growth rate for $t = 0^+$ will be approximately 0.4927.

3.3. *Transient behaviour*

Following the procedure described in §2.3, the temporal development of the maximum energy density growth has been calculated for various parameter combinations. Figure 4 shows the maximum energy amplification versus time for $\alpha = 0$, 0.1, and 1, a Reynolds number of $R = 3000$ and azimuthal wavenumbers $n = 1, 2, 3, 4$. For $\alpha = 0$ the ratio of energy density to the square of the Reynolds number is only dependent on the azimuthal wavenumber n, which has been exploited in figures 4(*a*) and 4(*b*). For non-zero streamwise wavenumbers this scaling breaks down due to the non-vanishing off-diagonal terms in (1*b*), and the temporal evolution of $G(\tau)$ has to be calculated for each individual Reynolds number.

The plots show a substantial amount of energy density amplification before an exponential decay sets in. Whereas the long-term behaviour is dominated by the least-stable eigenmode only, a *set* of eigenmodes is involved in the initial increase of energy density.

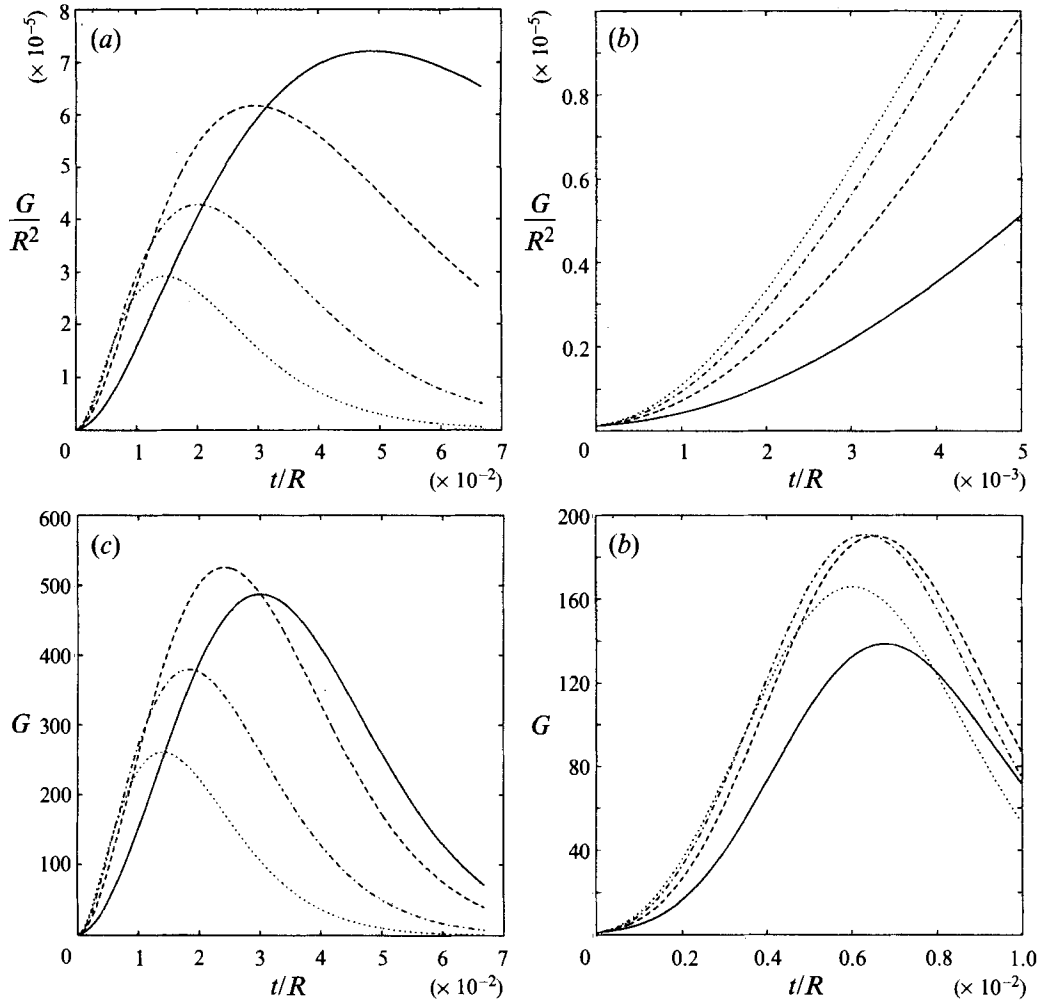

FIGURE 4. Transient growth versus time for circular pipe flow. (*a*) $\alpha = 0$, $n = 1, 2, 3, 4$, $R = 3000$; (*b*) close-up of (*a*) for small times; (*c*) $\alpha = 0.1$, $n = 1, 2, 3, 4$, $R = 3000$; (*d*) $\alpha = 1$, $n = 1, 2, 3, 4$, $R = 3000$. The solid line denotes $n = 1$, the dashed line $n = 2$, the chain dashed line $n = 3$ and the dotted line $n = 4$. For (*a*) and (*b*) the scaling of the growth function G by the square of the Reynolds number has been used which results in growth curves that are solely dependent on the azimuthal wavenumber n. In (*c*) and (*d*) the streamwise wavenumber α is non-zero and the same scaling does not apply.

This interesting result is best demonstrated by calculating the maximum of the growth curve G_{max} as a function of the number N of eigenfunctions included in the expansion (6). The eigenfunctions are sorted in descending order with respect to the imaginary part of the associated eigenvalue. The result is shown in figure 5.

If only one eigenfunction is included the maximum possible amplification factor G_{max} is one, which will be reached at time $\tau = 0$. This is due to the decaying nature of the pipe flow spectrum. After including about seven eigenfunctions the maximum possible amplification is nearly reached and varies by less than 1.2% if more eigenfunctions are included. Figure 5 thus demonstrates that transient growth of energy density is a multi-mode phenomenon.

A few important trends can be observed in figure 4. The increase of the streamwise wavenumber results in a more localized and less pronounced growth curve. This can

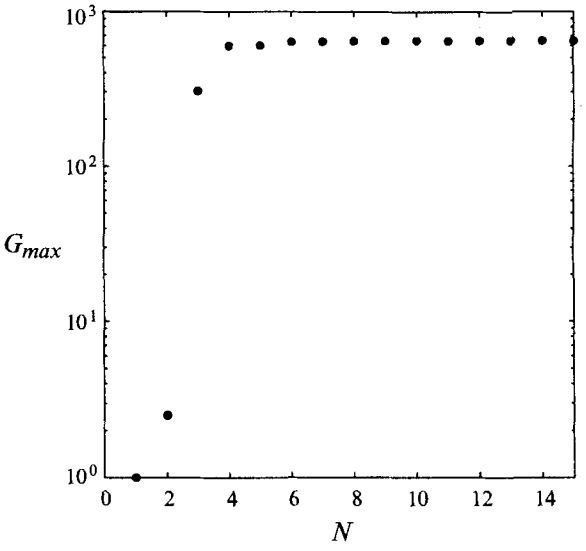

FIGURE 5. Dependence of the maximum amplification G_{max} on the number N of included eigenfunctions. The parameters are $\alpha = 0$, $n = 1$ and $R = 3000$.

be explained by the higher damping rates for fixed Reynolds number as α increases. During the initial rise in maximum energy density, waves with higher azimuthal periodicity dominate (see figure 4*b*). Another noteworthy characteristic of the growth curves is the fact that, for higher streamwise wavenumbers, disturbances that achieve the maximum amplification of initial energy are disturbances with increasingly higher azimuthal wavenumbers.

Axisymmetric disturbances ($n = 0$) experience a very small amount of transient growth and, therefore, have been omitted from the plots of figure 4.

Similar results to the ones presented in figure 4 have been found by Bergström (1992). He considers the growth of energy density that is associated with the streamwise velocity component normalized by the initial energy in the normal velocity only. Therefore, he reports larger amplification factors, which coincide with the ones given in figure 4 when properly scaled. In a subsequent paper (Bergström 1993) he computes the maximum transient growth employing the variational techniques used by Butler & Farrell (1992) with similar findings. For a wide range of parameters, O'Sullivan & Breuer (1992) also report large transient growth followed by exponential decay. Since their analysis is applied to a restricted class of initial conditions, the maximum possible amplification is less than the one shown in figure 4.

In addition to what has been done in the previous studies on transient growth in circular pipes (Boberg & Brosa 1988; O'Sullivan & Breuer 1992; Bergström 1992, 1993) we now present an exhaustive parameter study on the dependence of the transient growth on the governing parameters. First we investigate the dependence of the maximum amplification factor of initial energy density G_{max} on the Reynolds number and the streamwise and azimuthal wavenumbers. The results are displayed in figure 6 in the $(\alpha R, R)$-plane for four different azimuthal wavenumbers ($n = 0, 1, 2, 3$).

In the axisymmetric case (figure 6*a*) we observe an increasing value of G_{max} as αR becomes larger. A minimum value of $\alpha R \approx 369.7$, which has been found to be Reynolds-number independent for the values of R shown in figure 6(*a*), has to be exceeded in order to experience transient growth of energy density. Below this value the

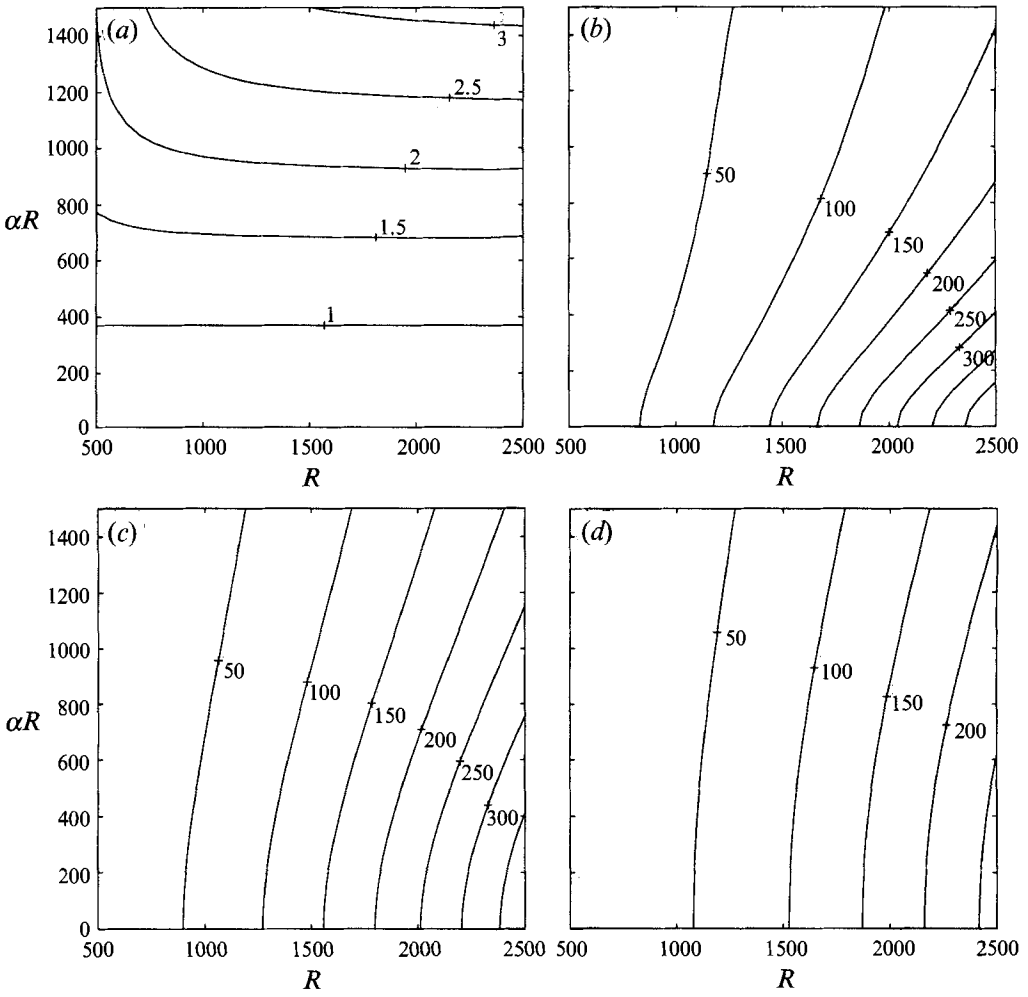

FIGURE 6. Contours of maximum transient growth in the $(\alpha R, R)$-plane for selected azimuthal wavenumbers. (*a*) Contours of G_{max} for $n = 0$, (*b*) $n = 1$, (*c*) $n = 2$, and (*d*) $n = 3$.

energy density exhibits decay for all times. The $G_{max} = 1$ contour is hence the curve that separates parameter combinations for which energy density growth may occur from ones for which energy density decay is assured.

The non-axisymmetric cases (figure 6*b–d*) differ qualitatively from the axisymmetric case. Figure 6(*b–d*) shows that the maximum possible amplification factor G_{max} is obtained for disturbances with vanishing streamwise wavenumber, i.e. for two-dimensional perturbations. A comparison between figures 6(*d*) and 6(*b*) reveals that for higher values of αR disturbances with higher azimuthal wavenumbers achieve larger values of G_{max} whereas for low αR the contrary is true. In figure 7 the ratio of maximum amplification factor of initial energy density G_{max} and the square of the Reynolds number R^2 is plotted. A vanishing dependence of this ratio on the Reynolds number for large R is observed which implies a quadratic scaling of the maximum energy density amplification with the Reynolds number as $R \to \infty$. Similar behaviour has been observed for plane Poiseuille and Couette flows (Reddy & Henningson 1993).

We will now determine the flow fields of assorted disturbances that will exploit the linear mechanism in an optimal way.

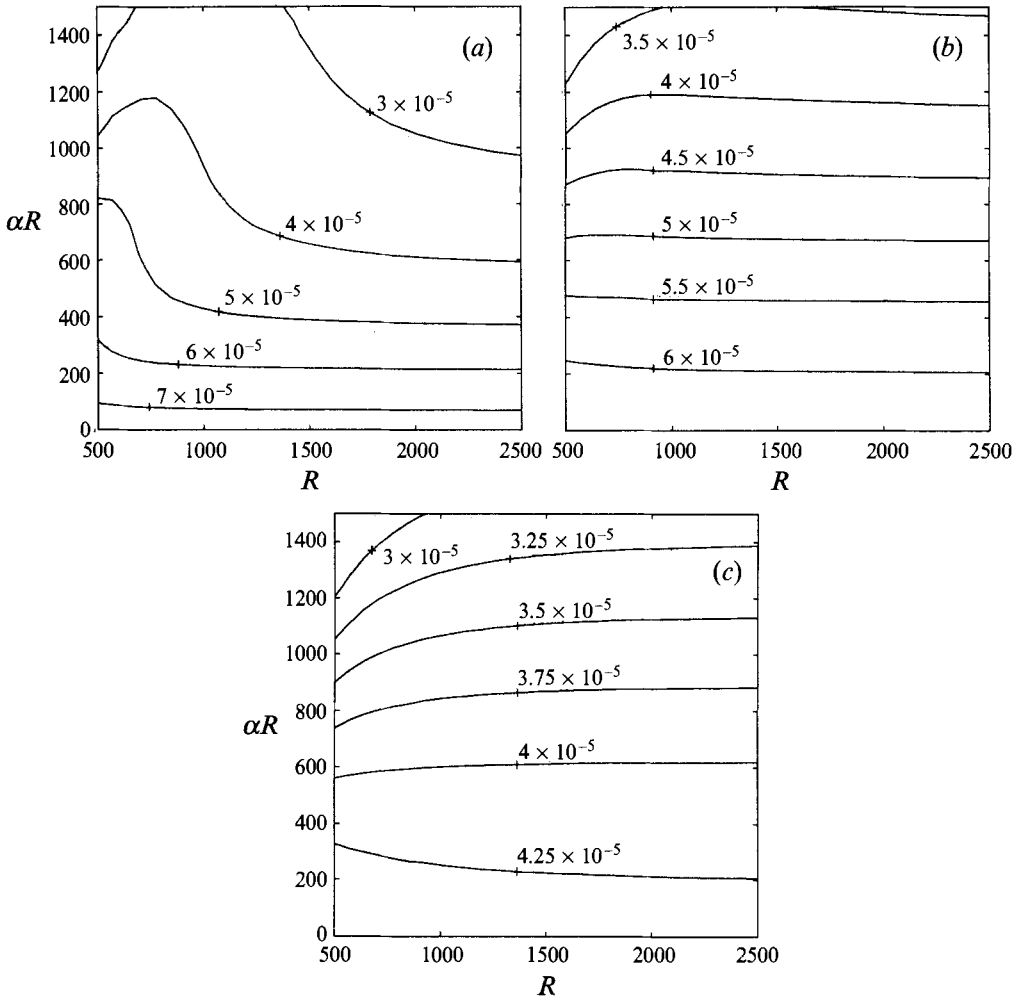

FIGURE 7. Contours of the ratio of maximum transient growth to the square of the Reynolds number G_{max}/R^2 in the $(\alpha R, R)$-plane for selected azimuthal wavenumbers. (*a*) Contours for $n = 1$, (*b*) $n = 2$, and (*c*) $n = 3$.

For this, we will first focus on two-dimensional ($\alpha = 0$) perturbations that have shown the largest possible amplification of their initial energy density content. A Reynolds number of $R = 3000$ and an azimuthal wavenumber of $n = 1$ have been chosen.

The initial condition that will result in a maximum amplification factor of 649 at a time $t_0 = 147$ is shown in figure 8(*a*). The velocity vectors in a cross-sectional (r, θ)-plane perpendicular to the streamwise coordinate axis are displayed. The flow field is characterized by a pair of strong counter-rotating vortices near the centre of the pipe which blend into a mostly azimuthal flow pattern as the pipe wall is approached. Figure 8(*b*) depicts the temporal evolution of energy density for this specific initial condition together with the maximum possible amplification (dotted curve), which for this specific case approximately coincide. Note that a non-zero radial perturbation velocity at the centre of the pipe is only possible for an azimuthal wavenumber of $n = 1$. Disturbances with higher azimuthal periodicity as well as axisymmetric perturbations will leave the mean centreline velocity unperturbed.

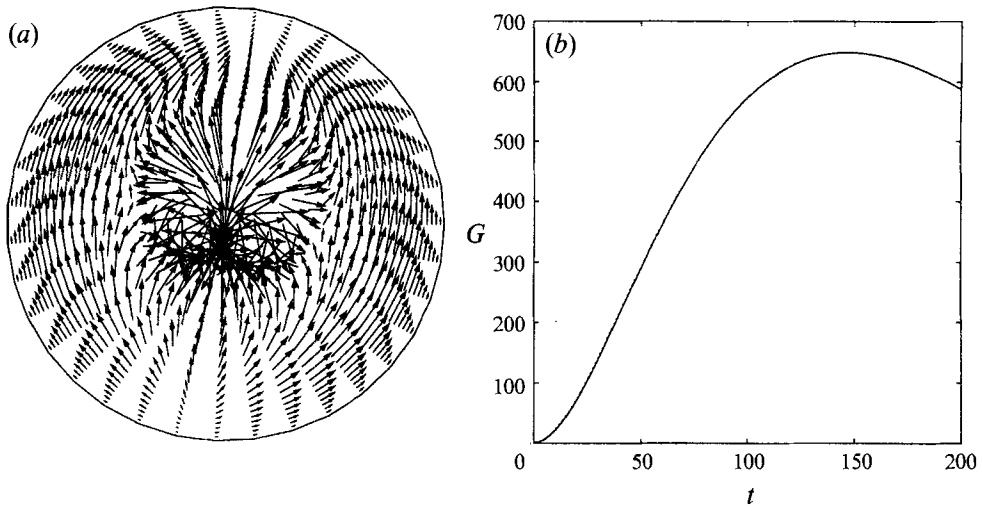

FIGURE 8. (*a*) Vector flow field of the optimal perturbation in the (r, θ)-plane for $\alpha = 0, n = 1, R = 3000$ and $t_0 = t_{opt}$ and (*b*) its individual (solid) and optimal (dotted) growth curve. For this case, the two growth curves coincide within plotting accuracy.

To investigate the dependence on the time t_0 at which the perturbation reaches its maximum possible energy amplification, an initial disturbance has been computed that will reach its optimal amplification at a chosen time of $t_0 = 2$. Recall that at time $t = t_0$ the curve displaying the energy density of this particular initial disturbance will be tangent to the maximum growth curve. This is shown in figure 9(*b*). The flow field of the initial disturbance (figure 9*a*) is remarkably similar to the one in figure 8(*a*). The temporal evolution of the energy density for this initial condition is still close to the optimal curve, reaching more than 90% of the optimal energy density amplification, although tangency at $t_0 = 2$ is enforced. This leads us to the conclusion that for two-dimensional disturbances with $n = 1$ the shape of the optimal initial perturbation is of rather universal type and insensitive to the details of the linear growth characteristics such as the choice of t_0. This finding has not been observed for flows in plane geometries, such as Poiseuille and Couette flow (Reddy & Henningson 1993). In this case, the choice of t_0 such that $t_0 < t_{max}$, where t_{max} denotes the time at which G_{max} is reached, resulted in initial disturbances that were more and more concentrated in the wall region as t_0 decreased. As has been pointed out by Trefethen *et al.* (1993), other optimal perturbations are conceivable, such as the disturbance that exhibits the largest initial growth or the perturbation that maximizes the resonant response to an external forcing. The investigation of these structures is outside the scope of our study.

The two cases considered above had no streamwise variation. For comparison, we also computed the structure of a three-dimensional initial condition with a streamwise wavenumber of $\alpha = 1$. For this case, the time t_0 has been chosen as $t_0 = 10$. The flow field of the initial disturbance (figure 9*c*) is substantially different from the previous cases (figures 8*a* and 9*a*). An overall swirling structure can be detected that, together with the axial flow components, suggests a strongly helical fluid motion.

3.4. *Conditions for no growth*

We conclude this investigation of transient growth in circular pipe flow with a computation of the boundaries in parameter space below which any transient growth in energy density can be ruled out. To accomplish this we use the concept of the

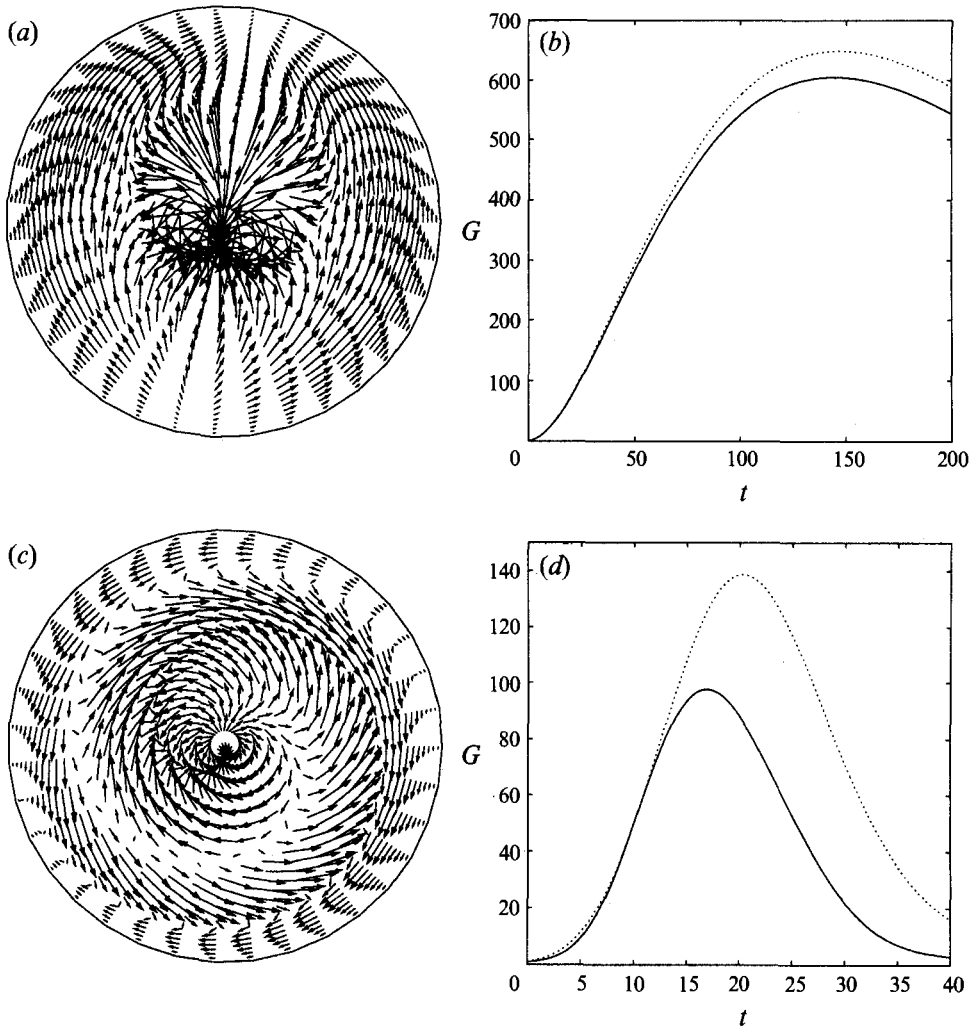

FIGURE 9. Vector flow fields of the optimal perturbations in the (r, θ)-plane for (*a*) $\alpha = 0$, $n = 1$, $R = 3000$ and $t_0 = 2$ and (*b*) its individual (solid) and optimal (dotted) growth curve; and (*c*) for $\alpha = 1$, $n = 1$, $R = 3000$ and $t_0 = 10$ and (*d*) its individual (solid) and optimal (dotted) growth curve.

numerical range introduced in §2.5 and determine (α, R)-pairs for selected azimuthal wavenumbers for which the maximum imaginary part of the boundary of the numerical range is zero. According to (13), this will give the curves in the (α, R)-plane that separate regions of initial energy density growth from regions of initial energy density decay. The curves are shown in figure 10 and are found to be equivalent to the energy stability boundaries obtained in Joseph & Carmi (1969) by a variational technique. It is worth pointing out that the energy stability results (Joseph & Carmi 1969) are nonlinear stability results. The equivalence between the energy stability results and the results obtained from calculating the numerical range is because the nonlinear terms of the Navier–Stokes equations are energy conserving and thus allow the growth or decay of perturbation energy to be treated by the linear theory. The curve resulting in the lowest Reynolds number for energy stability is associated with an azimuthal wavenumber of $n = 1$ and the critical parameter combination has been computed as

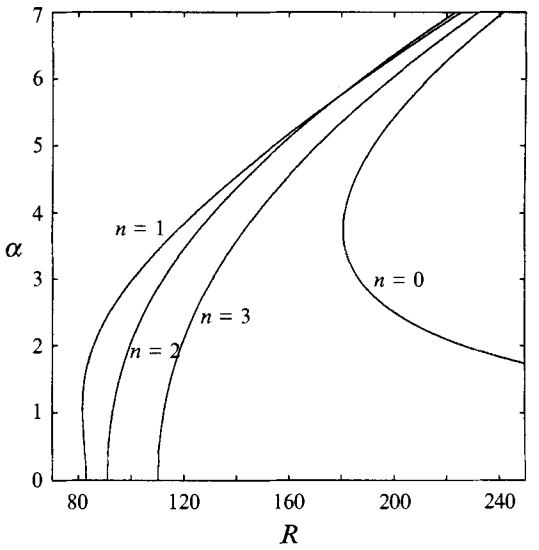

FIGURE 10. Boundaries separating regions of initial energy density growth from regions of initial energy density decay in the (α, R)-plane for various azimuthal wavenumbers.

$\alpha = 1.07$, $R = 81.49$, which conforms with the results reported in Joseph & Carmi (1969).

4. Summary and conclusions

The stability of incompressible viscous fluid flow in a circular pipe to infinitesimal three-dimensional disturbances has been considered. Both the flow stability for asymptotically large times governed by the eigenvalues and transient effects associated with the non-normality of the linearized stability operator have been investigated in detail. A formulation of the governing equations in terms of the radial velocity and radial vorticity has been used in conjunction with an expansion in the eigenfunctions of the linearized problem. Mathematical tools introduced in Reddy *et al.* (1993) and Reddy & Henningson (1993) have been adapted to the circular geometry and have subsequently been applied to determine the behaviour of solutions to the linear initial-value problem.

Concerning the asymptotic stability of flows in circular pipes described by the spectrum of the linearized evolution operator, a family of modes reported by Davey & Drazin (1969) has been identified as a numerical artifact resulting from an insufficient resolution of modes with higher damping rates.

Large transient growth preceding the exponential decay has been found which is largest for disturbances with azimuthal wavenumber $n = 1$ and vanishing streamwise dependence, in agreement with other investigators (O'Sullivan & Breuer 1992; Bergström 1992, 1993). The short-time behaviour, however, is dominated by perturbations with higher azimuthal periodicities. The largest possible amplification of initial energy density is monotonically increasing with Reynolds number, showing a quadratic Reynolds-number dependence as $R \to \infty$. The flow fields for the optimal initial disturbance have been determined for selected parameter combinations, resulting in a pair of counter-rotating vortices near the centreline embedded in a strongly azimuthal fluid motion near the wall for $\alpha = 0$. For $\alpha = 1$, the optimal disturbance

consists of a swirling flow field leading to an overall helical motion. Finally, the curves in parameter space, limiting the growth of energy density, have been determined by computing the numerical range of the linear stability operator. These curves have been found to coincide with the stability boundaries given by the energy method (Joseph & Carmi 1969).

The above study has revealed both similarities and discrepancies between transient effects in pipe and other shear flows. The largest transient amplification of initial disturbance energy has been observed for perturbations with vanishing streamwise dependence in accordance with plane shear flows (see Butler & Farrell 1992; Reddy & Henningson 1993). The insensitivity of the optimal disturbances for $\alpha = 0$ to the choice of time t_0 at which they reach their maximum amplification factor, on the other hand, has not been observed in plane shear flows. Also, the maximum possible growth G_{max} has been obtained by including only a few modes in the eigenfunction expansion, a fact that does not have an analogue in plane shear flows. Besides these discrepancies, the results for the circular pipe geometry are qualitatively similar to the ones obtained for plane shear flows.

The linear growth mechanism described has been shown to operate on a fast timescale with amplification factors that can result in energies well within the range of nonlinear effects. This mechanism may therefore constitute a fundamental component of a rapid transition scenario in a low-energetic disturbance environment. As only a linear mechanism has been shown to generate a net gain in total disturbance energy, but fails to sustain turbulent fluid motion, a combination of the linear transient growth process studied in this paper and a nonlinear energy distribution process is proposed as the underlying mechanism for the transition to turbulence in circular pipe flow. The work of Boberg & Brosa (1988) suggests such a combination of linear and nonlinear mechanisms in the transition to turbulence in a pipe. Although further investigations in this direction are warranted, their results are indeed promising in explaining the underlying mechanisms for the onset of turbulence in a circular pipe. It is believed that the linear mechanism described in this presentation will play a dominant role during transition. An investigation of this matter is left for a future effort.

Support for the first author has been provided by an Alfred P. Sloan Foundation Doctoral Dissertation Award. Computer time has been provided by NCSA, Urbana-Champaign.

Appendix

As an aid to the reader unfamiliar with the mathematical tools employed in §2, a simple 2×2 model problem will be discussed that illustrates the need for non-modal analysis and demonstrates the mathematical means to quantify transient effects.

A linear evolution equation of the form

$$\frac{\mathrm{d}}{\mathrm{d}t}\begin{pmatrix} v \\ \eta \end{pmatrix} = \begin{pmatrix} -\dfrac{1}{R} & 0 \\ 1 & -\dfrac{2}{R} \end{pmatrix}\begin{pmatrix} v \\ \eta \end{pmatrix} \tag{A 1}$$

is taken, where v and η resemble the normal velocity and normal vorticity respectively, and R denotes an equivalent Reynolds number. The influence of the velocity on the vorticity is accounted for by the off-diagonal term in the evolution operator. The weak

viscous coupling between velocity and vorticity (see main text) has however been neglected. As will be shown below, the above equation mimics many of the features of the more complicated evolution problem for flow in circular pipes as discussed in §2. The same model equation has been proposed by Trefethen *et al.* (1993) to illustrate the importance of non-modal behaviour in plane wall-bounded shear flows.

It is straightforward to determine the eigenvalues and normalized eigenvectors of the model equation as

$$\lambda_1 = -1/R, \quad \boldsymbol{\Phi}_1 = \frac{1}{(1+R^2)^{1/2}}\begin{pmatrix}1\\R\end{pmatrix},$$

$$\lambda_2 = -2/R, \quad \boldsymbol{\Phi}_2 = \begin{pmatrix}0\\1\end{pmatrix},$$

and the complete solution expanded in an eigenvector basis can be written as

$$\begin{pmatrix}v\\\eta\end{pmatrix} = \frac{A}{(1+R^2)^{1/2}}\begin{pmatrix}1\\R\end{pmatrix}e^{-t/R} + B\begin{pmatrix}0\\1\end{pmatrix}e^{-2t/R}. \tag{A 2}$$

The constants A and B are determined from the initial conditions.

It is immediately apparent from the sign of the eigenvalues that in the asymptotic limit of large time, the velocity and vorticity will decay to zero, independent of the initial conditions. On a shorter timescale, no conclusions can be drawn from the eigenvalues alone, and we need to resort to more appropriate tools.

Writing the evolution equation (A 1) in the compact form

$$\frac{\mathrm{d}}{\mathrm{d}t}\boldsymbol{q} = \boldsymbol{A}\boldsymbol{q}$$

we can write the formal solution to the initial value problem as

$$\boldsymbol{q}(t) = e^{t\boldsymbol{A}}\boldsymbol{q}_0,$$

with $\boldsymbol{q}_0$ as the vector consisting of the initial velocity and vorticity. As a measure of maximum growth we define the growth function $G(t)$ as the square of the L_2-norm of the disturbance, i.e. $\|\boldsymbol{q}\|^2 = v^2+\eta^2$, normalized by the initial disturbance norm, and optimized over all initial conditions. Mathematically, this means

$$G(t) = \sup_{\boldsymbol{q}_0}\frac{\|\boldsymbol{q}(t)\|^2}{\|\boldsymbol{q}_0\|^2} = \sup_{\boldsymbol{q}_0}\frac{\|e^{t\boldsymbol{A}}\boldsymbol{q}_0\|^2}{\|\boldsymbol{q}_0\|^2} = \|e^{t\boldsymbol{A}}\|^2.$$

The matrix exponential for (A 1) takes the form

$$e^{t\boldsymbol{A}} = \begin{pmatrix} e^{-t/R} & 0 \\ -(e^{-2t/R}-e^{-t/R})\,R & e^{-2t/R}\end{pmatrix},$$

and its L_2-norm versus time is plotted in figure 11 (*a*) for different values of the Reynolds number R. As can be seen, substantial transient growth can result before the asymptotic behaviour governed by the (least-damped) eigenvalue prevails.

It should be noted that the transient amplification is due to the increase in the vorticity component. The velocity component is decaying monotonically, as can be seen by looking at the velocity component of (A 2). The decaying velocity is, however, forcing the vorticity, which then results in transient growth.

The reason for the large transient growth of the disturbance norm lies in the non-normal nature of the evolution operator $\boldsymbol{A}$, i.e. $\boldsymbol{A}^T\boldsymbol{A} \neq \boldsymbol{A}\boldsymbol{A}^T$, which results in a set of

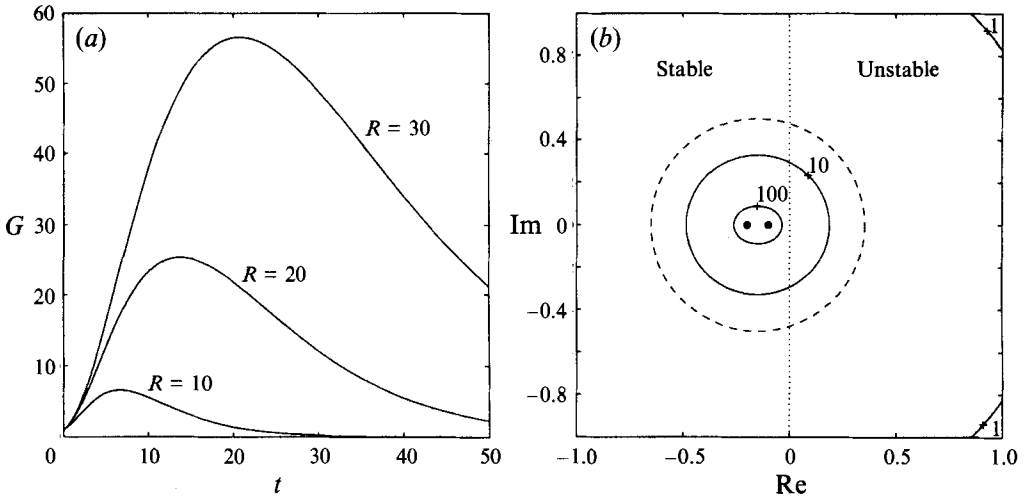

FIGURE 11. (*a*) Transient amplification of initial disturbance norm versus time for selected Reynolds numbers $R = 10, 20, 30$; (*b*) contours of the resolvent norm, boundary of the numerical range (dashed line) and spectrum (symbols) of $\boldsymbol{A}$ for $R = 10$.

non-orthogonal eigenvectors $\boldsymbol{\Phi}_1$ and $\boldsymbol{\Phi}_2$. The angle ϕ between the eigenvectors can be determined as

$$\phi = \arccos\left(\frac{R}{(1+R^2)^{1/2}}\right),$$

which rapidly approaches zero as the Reynolds number R increases, thus leading to an increasingly ill-conditioned expansion basis (see (A 2)) and to large transient growth (figure 11).

Figure 11(*a*) shows that the transient amplification of the initial disturbance norm is dependent on the Reynolds number R. To investigate this dependence further, it is instructive to consider the evolution equation for the disturbance norm. We have

$$\frac{\mathrm{d}}{\mathrm{d}t}\|\boldsymbol{q}\|^2 = 2\boldsymbol{q}^T\frac{\mathrm{d}}{\mathrm{d}t}\boldsymbol{q} = 2\boldsymbol{q}^T\boldsymbol{A}\boldsymbol{q} = -\frac{2(2v^2+\eta^2)}{R} + 2v\eta,$$

where $\|\boldsymbol{q}\| = 1$ has been assumed.

Defining the numerical range of $\boldsymbol{A}$ as

$$\mathscr{F}(\boldsymbol{A}) = \{z \in \mathscr{C} : z = \boldsymbol{x}^H\boldsymbol{A}\boldsymbol{x} \quad \text{with} \quad \boldsymbol{x} \in \mathscr{C}^2 \quad \text{and} \quad \|\boldsymbol{x}\| = 1\},$$

we can use this quantity to determine the initial growth of the disturbance $\boldsymbol{q}$ in the L_2-norm. In analogy to the results shown in §2.5, the largest real value of the numerical range $\mathscr{F}_{max}$ is equivalent to half the slope of the growth function $G(t)$ at $t = 0$. The expression for $\mathscr{F}_{max}$ in our case can be derived as

$$\mathscr{F}_{max} = -\frac{1}{2R}\left(3 - \frac{1}{(1+R^2)^{1/2}}\right) + \frac{R}{2(1+R^2)^{1/2}} = \frac{1}{2}\frac{\mathrm{d}G}{\mathrm{d}t}\bigg|_{t=0}.$$

The Reynolds number R_g, which renders $\mathscr{F}_{max}$ equal to zero, is thus equivalent to the Reynolds number below which no transient growth can be expected. For our model problem, a straightforward calculation shows that

$$R_g = \sqrt{8} \quad \text{and therefore} \quad \frac{\mathrm{d}G}{\mathrm{d}t} < 0 \quad \text{for} \quad R < \sqrt{8}.$$

As has been pointed out, the eigenvalues of our model only determine the asymptotic behaviour of the solutions to the initial-value problem. To capture the short-time behaviour, we need to introduce the notion of ϵ-pseudospectra which (for matrices) is given as:

A number $z \in \mathscr{C}$ lies in the ϵ-pseudospectrum of a matrix $\boldsymbol{A}$, if $\|(z\boldsymbol{I}-\boldsymbol{A})^{-1}\| \geqslant \epsilon^{-1}$.

For our model problem the quantity $(z\boldsymbol{I}-\boldsymbol{A})^{-1}$, known as the resolvent, is given as

$$(z\boldsymbol{I}-\boldsymbol{A})^{-1} = \begin{pmatrix} \dfrac{R}{zR+1} & 0 \\ \dfrac{R^2}{(zR+1)(zR+2)} & \dfrac{R}{zR+2} \end{pmatrix}.$$

For normal evolution operators, the contours of the resolvent norm are ϵ-balls about the eigenvalues, whereas for non-normal operators the contours enclose larger regions of the complex plane. The contours of the resolvent norm together with the spectrum and the numerical range are depicted in figure 11(*b*). The contours clearly demonstrate the non-normal nature of the evolution operator. The norm of the resolvent can be used to calculate upper and lower bounds on the maximum growth $G_{max} = \sup_{t \geqslant 0} G(t)$. For details the reader is referred to Reddy *et al.* (1992).

In summary, the analysis of this model problem demonstrates that special care is warranted when analysing the stability characteristics of linear evolution problems based on non-normal operators. Eigenvalues only govern the asymptotic time behaviour in this case, and the norm of the matrix exponential and the numerical range have to be calculated to draw conclusions about the short-time behaviour of the system and about conditions for the occurrence of transient effects. All of these features are discussed in the main text for the case of disturbance evolution in incompressible circular pipe flow.

REFERENCES

BERGSTRÖM, L. 1992 Initial algebraic growth of small angular dependent disturbances in pipe Poiseuille flow. *Stud. Appl. Maths* **87**, 61–79.

BERGSTRÖM, L. 1993 Optimal growth of small disturbances in pipe Poiseuille flow. *Phys. Fluids* A **5**, 2710–2720.

BOBERG, L. & BROSA, U. 1988 Onset of turbulence in a pipe. *Z. Naturforsch.* **43a**, 697–726.

BURRIDGE, D. M. & DRAZIN, P. G. 1969 Comments on 'Stability of pipe Poiseuille flow'. *Phys. Fluids* **12**, 264–265.

BUTLER, K. M. & FARRELL, B. F. 1992 Three-dimensional optimal perturbations in viscous shear flow. *Phys. Fluids* A **4**, 1637–1650.

DAVEY, A. 1978 On the stability of flow in an elliptic pipe which is nearly circular. *J. Fluid Mech.* **87**, 233–241.

DAVEY, A. & DRAZIN, P. G. 1969 The stability of Poiseuille flow in a pipe. *J. Fluid Mech.* **36**, 209–218.

DAVEY, A. & NGUYEN, H. P. F. 1971 Finite-amplitude stability of pipe flow. *J. Fluid Mech.* **45**, 701–720.

DIPRIMA, R. C. 1967 Vector eigenfunction expansions for the growth of Taylor vortices in the flow between rotating cylinders. In *Nonlinear Partial Differential Equations* (ed. W. F. Ames). Academic.

DRAZIN P. G. & REID, W. H. 1981 *Hydrodynamic Stability*. Cambridge University Press.

FARRELL, B. F. 1988 Optimal excitation of perturbations in viscous shear flow. *Phys. Fluids* **31**, 2093–2102.

GUSTAVSSON, L. H. 1989 Direct resonance of nonaxisymmetric disturbances in pipe flow. *Stud. Appl. Maths* **80**, 95–108.

GUSTAVSSON, L. H. 1991 Energy growth of three-dimensional disturbances in plane Poiseuille flow. *J. Fluid Mech.* **224**, 241–260.

HENNINGSON, D. S. & REDDY, S. C. 1994 On the role of linear mechanisms in transition to turbulence. *Phys. Fluids* **6**, 1396–1398.

HENNINGSON, D. S. & SCHMID, P. J. 1992 Vector eigenfunction expansions for plane channel flows. *Stud. Appl. Maths* **87**, 15–43.

HERBERT, T. 1977 Die neutrale Fläche der ebenen Poiseuille Strömung. Habilitationsschrift, Universität Stuttgart.

HERRON, I. 1991 Observations on the role of vorticity in the stability theory of wall bounded flows. *Stud. Appl. Maths* **85**, 269–286.

HORN, R. & JOHNSON, J. 1991 *Topics in Matrix Analysis*. Cambridge University Press.

HOWARD, L. N. & GUPTA, A. S. 1962 On the hydrodynamic and hydromagnetic stability of swirling flows. *J. Fluid Mech.* **14**, 463–476.

JOSEPH, D. D. & CARMI, S. 1969 Stability of Poiseuille flow in pipes, annuli and channels. *Q. Appl. Maths* **26**, 575–591.

KATO, T. 1976 *Perturbation Theory for Linear Operators*. Springer.

KHORRAMI, M. R., MALIK, M. R. & ASH, R. L. 1989 Application of spectral collocation techniques to the stability of swirling flows. *J. Comput. Phys.* **81**, 206–229.

LESSEN, M., SADLER, S. G. & LIU, T.-Y. 1968 Stability of pipe Poiseuille flow. *Phys. Fluids* **11**, 1404–1409.

LUNDBLADH, A. 1993 Simulation of bypass transition to turbulence in wall bounded shear flows. PhD thesis, Department of Mechanics, KTH, Stockholm.

MACKRODT, P.-A. 1976 Stability of Hagen–Poiseuille flow with superimposed rigid rotation. *J. Fluid Mech.* **73**, 153–164.

MASLOWE, S. A. 1974 Instability of rigidly rotating flows to non-axisymmetric disturbances. *J. Fluid Mech.* **64**, 307–317.

METCALFE, R. & ORSZAG, S. A. 1973 Numerical calculations of the linear stability of pipe flow. *Flow Research Rep.* 25. Kent Washington.

O'SULLIVAN, P. L. & BREUER, K. S. 1992 Transient growth of non-axisymmetric disturbances in laminar pipe flow. *Technical Rep., Center for Fluid Dynamics, Brown University.*

PAZY, A. 1983 *Semigroups of Linear Operators and Applications to Partial Differential Equations*. Springer.

REDDY, S. C. & HENNINGSON, D. S. 1993 Energy growth in viscous channel flow. *J. Fluid Mech.* **252**, 209–238.

REDDY, S. C., SCHMID, P. J. & HENNINGSON, D. S. 1993 Pseudospectra of the Orr–Sommerfeld operator. *SIAM J. Appl. Maths* **53**, 15–45.

ROMANOV, V. A. 1973 Stability of plane-parallel Couette flow. *Funkcional Anal. i Prolozen.* **7** (2), 62–73. (Translated in *Functional Anal. & Applics.* **7**, 137–146.)

SALWEN, H., COTTON, F. W. & GROSCH, C. E. 1980 Linear stability of Poiseuille flow in a circular pipe. *J. Fluid Mech.* **98**, 273–284.

TATSUMI, T. 1952 Stability of the laminar inlet-flow prior to the formation of Poiseuille regime, II. *J. Phys. Soc. Japan* **7**, 495.

TREFETHEN, L. N. 1992 Pseudospectra of matrices. In *Numerical Analysis* 1991 (ed. D. F. Griffiths & G. A. Watson). Longman.

TREFETHEN, L. N., TREFETHEN, A. E., REDDY, S. C. & DRISCOLL, T. A. 1993 Hydrodynamic stability without eigenvalues. *Science* **261**, 578–584.

WILLKE, L. H. 1967 Stability in time-symmetric flows. *J. Math. Phys.* **46**, 151–163.